NTNU
Norwegian University of Science and Technology

On-Line Voltage Stability Assessment

Combining Model Based and Measurement Based Indicators .

Vilde Rye-Holmboe

Preface

This work is a contribution to the field of on-line voltage stability assessment and looks into how model and measurement based methods can be combined. This master thesis is a result of a specialisation project conducted in the fall of 2016 and further study during the spring of 2017. The work was carried out at the Department of Electric Power Engineering, as part of fulfilling the requirements of the Energy and Environmental Engineering program at the Norwegian University of Science and Technology (NTNU).

I first became interested in issues concerning system stability during my exchange stay at Danmarks Teknikske Universitet (DTU) in 2015, and I became determined to write my master thesis on this topic. What I find interesting about power system stability is that there are no simple answers and no simple solutions, when dealing with these types of problems.

A lot of the work on this project has included programming in Python and MATLAB, to make an appropriate case study and to implement the methods. Being a novice to both Python and PSS/E, many hours have been spent to acquire the necessary programming skills. I have learnt that theory and reality do not always coincide, which can be frustrating when you are a perfectionist like me. All in all, this have been an enjoyable experience, leaving me with more questions than answers, but that is what learning is all about I suppose.

I would like to thank my supervisor Professor Kjetil Uhlen, for his guidance and helpful suggestions during the work on this thesis. Also, I want to thank PostDoc Dinh Thuc Duong, for his help in regards to the theoretical background of the S-Z sensitivity indicator, and implementation of it. Lastly, I would like to thank my boyfriend and my parents for encouraging and supporting me through these last five years.

Vilde Rye-Holmboe
Trondheim, 17th June 2017

Abstract

This master thesis has examined the possibility of combining measurement and model based methods for on-line voltage stability assessment in the power system. Voltage instability may lead to voltage collapse and blackout of total or parts of the system. To avoid severe damage to equipment, disconnection of customers and the resulting economic costs it is significant to know how far the system is from the stability limit. It is desirable that the system operator is warned as soon as possible when the system approaches the stability limit so that he/she has time to initiate countermeasures.

The maximum loadability of the transmission grid has been found to be a good indicator of voltage stability. A proposed method combining *Continuation Power Flow* (CPF) and the *S-Z Sensitivity Indicator* (S-ZI) has been presented and implemented in a case study where a power system approaches voltage collapse, through a series of consecutive disturbances. The CPF is based on a system model and requires measurements from the whole system (provided by the State Estimator (SE)). It finds a continuum of power flow solutions at the load bus to find the maximal loadability, which makes it computational demanding to carry through. Since it uses a model of the whole system, it is possible to simulate potential outages in the system, to study the steady-state stability after contingencies. The S-ZI uses measurements from the Phasor Measurement Unit (PMU), placed at the load bus. The S-ZI needs few measurements, is easy to compute and can, therefore, be conducted more frequently than the CPF.

The master thesis proposes a new method that aims to combine the accuracy of the CPF, with the frequency of the S-ZI. By combining the resulting maximum loadability estimated by the S-ZI (computed every 40 ms), which is then corrected by the CPF (computed every 5 minutes), the proposed method finds a new maximum loadability of the system, $P_{MAX,REAL}$.

The proposed method was able to detect that the system had moved into the alert state after the system had been subjected to a contingency. Based on the results of the case study, it is not, however, possible to conclude that the actual maximum loadability of the system have been found by the proposed method.

Both the S-ZI and the CPF were found to overestimate the maximum loadability of the system. Particularly the maximum loadability estimated by the S-ZI was found to vary a lot, overestimating the maximum loadability limit by as much as 2-3 times compared to the actual limit at some time steps. The variation in the resulting $P_{MAX,S-ZI}$ is too big to give any real information about the change in the maximum loadability between every time the CPF is solved. The results of the case study show that the proposed method can, at best, provide an indication of where the system is headed. Further study is needed to find a more appropriate monitoring of the actual variation of the maximum loading limit in the system.

Sammendrag

Denne masteroppgaven har undersøkt hvordan måle- og modellbaserte metoder kan kombineres for å evaluere on-line spenningsstabilitet i strømnettet. Ustabilitet i spenning kan føre til spenningskollaps eller strømbrudd i hele eller store deler av strømnettet. For å unngå alvorlig ødeleggelse på utstyr, utkobling av kunder og de resulterende økonomiske kostnadene dette medfører er det viktig å vite hvor langt systemet er fra stabilitetsgrensen. Det er ønskelig at systemoperatøren blir varslet så snart systemet nærmer seg stabilitetsgrensen, slik at han/hun har tid til å sette i gang mottiltak.

Den maksimale overføringskapasitet til systemet har vist seg å være en god indikator for spenningsstabiliteten i nettet. En ny metode som kombinerer *Continuation Power Flow* (CPF) og *S-Z sensitivitetsindikator* (S-ZI) har blitt presentert og anvendt på et case studie, der systemet nærmer seg en spenningskollaps gjennom en serie utfall i nettet, for å finne den maksimale overføringskapasiteten. CPF er basert på en systemmodell og tar inn målinger fra hele nettet (fra tilstandsestimatoren (SE)). Den finner et kontinuum av lastflytløsninger, for å finne maksimal overføringskapasitet til lasten. Behovet for mange steg gjør metoden krevende å gjennomføre beregningsmessig. Siden metoden bruker en modell av systemet er det mulig å gjøre endringer, for å simulere potensielle utfall i systemet og den resulterende stajonære spenningsstabiliteten i nettet. S-ZI bruker målinger fra *Phasor Measurment Unit* (PMU) plassert på lastbussen. S-ZI trenger få målinger, er enkel å beregne, og kan derfor foretas mye oftere en CPF.

Denne masteroppgaven foreslår en ny metode som forsøker å kombinere nøyaktigheten i beregningene fra CPF, med hyppigheten av målinger fra SZ-I. Ved å kombinere den maksimale overføringskapasiteten beregnet fra S-ZI (beregnet hvert 40 ms), som blir korrigert med resultatet fra CPF (beregnet hvert femte minutt), forsøker den foreslåtte metoden å finne en ny maksimal overføringskapasitet i systemet, $P_{MAX,REAL}$.

Den foreslåtte metoden klarte å detektere at systemet hadde gått inn i *alert state* etter driftsstans av generatoren. Basert på resultatene fra case studiet, er det ikke mulig å konkludere at den faktiske maksimale overføringskapasiteten til systemet har blitt funnet ved hjelp av metoden. Både S-ZI og CPF overestimerte maksimal overføringskapasitet til systemet.

Den maksimale overføringskapasitet beregnet fra S-ZI varierer spesielt mye, og er opp til 2-3 ganger så høy som den faktiske ved enkelte tidssteg. Variasjonen i den beregnede $P_{MAX,S-ZI}$ er for stor til å gi pålitelig informasjon om variasjonen i maksimal overføringskapasitet mellom hver gang CPF blir gjennomført. Resultatet fra case studiet antyder at den foreslåtte metoden i beste fall kan gi en indikasjon for hvor systemet er på vei. Videre undersøkelser er nødvendig for å finne en bedre egnet overvåking av den faktiske variasjonen i maksimal overføringskapasiteten i strømnettet.

Contents

List of Figures

List of Tables

Abbreviations

AVR	Automatic Voltage Regulator
CPF	Continuation Power Flow
DSA	Dynamic Security Assessment
EMS	Energy Management System
EXTL	Extended-Term Load Reset
FACTS	Flexible AC Transmission System
FC	Fixed Capacitor
GPS	Global Positioning System
IED	Intelligent Electronic Device
OLTC	On-line load tap changing
OPF	Optimal power flow
OXL	Overexcitation Limiter
PDC	Phasor Data Concentrator
PMU	Phasor Measurement Unit
RTU	Remote Terminal Unit
SCADA	Supervisory Control and Data Acquisition
SE	State Estimator
STATCOM	Static Compensator
SSA	Static Security Assessment
SSSC	Static Synchronous Series Compensator
SVC	Static VAR Compensator
S-ZI	S-Z Sensitivity Indicator
TCR	thyristor-controlled reactor
TSC	thyristor-switched capacitor
TSR	thyristor-switched reactor
UTC	Universal Time Coordinated
UPFC	Unified Power Flow Controllers
WAMS	Wide Area Monitoring System

Nomenclature

$\vec{E}_{Th}$	Thevenin voltage
$\vec{I}$	Current
P	Active power
S	Apparent power magnitude, $S = \sqrt{P^2 + Q^2}$
$\vec{S}$	Apparent power, $\vec{S} = P + jQ$
Q	Reactive power
$\vec{V}$	Voltage, $\vec{V} = |V| \angle \delta$
θ	Angle between $\vec{Z}_{Th}$ and $\vec{Z}_L$
$\vec{Z}_{Th}$	Thevenin impedance, $\vec{Z}_{Th} = Z_{Th} \angle \alpha = R_{Th} + jX_{Th}$
$\vec{Z}_L$	Load impedance, $\vec{Z}_L = Z_L \angle \phi = R_L + jX_L$
δ	Voltage angle
ζ	S-ZI, $\zeta = dS_L/dZ_L$
α	Phase angle of Thevenin impedance
ϕ	Phase angle of load impedance
k_{PV}, k_{QV}	Voltage sensitivities of the load (slope of active and reactive power demand characteristics as a function of voltage V)

1 | Introduction

This master thesis is the result of a literature review conducted during the fall of 2016, for the specialisation project on the same topic, and further work during the spring of 2017. First, this introductory part will address the background and motivation for looking into on-line stability assessment. Then the objectives, scope and limitations of the work will be outlined, and the structure of the thesis will be presented with emphasis on the intention of each part. Some of the theory is based on the findings from the specialisation project, and this will, therefore, be accounted for in the last part of this introduction. Clarification on some terms that will frequently be used throughout this report will be given at the end.

1.1 Background and Motivation

Voltage instability has come forth as one of the major threats against secure system operation. Voltage instability in power systems can in the worst case lead to voltage collapse or blackouts. The voltage level and the reactive power reserve in the system have been shown to be poor indicators for voltage instability [8]. Voltage instability is often related to the maximum loadability of the transmission network. Therefore, it is crucial that the system operator knows how far the system is from its maximum loading limit. The maximum loading limit is not a fixed quantity as the power system is subjected to changes continuously, due to changes in power demand, power production and due to planned and unplanned outages.

For the system operator, it is important to ensure a secure operation of the power system and provide a continuous power supply to the costumers. System monitoring gives the system operator an indication of the current operating state of the system. An early warning about events, driving the system towards the stability limit, may enable the system operator to set in remedial and corrective actions to avoid instability.

Monitoring of the power system has become more important in the last few decades. There have been two major paradigm shifts, which have affected the energy systems a lot. Many countries have liberalised the power market, to improve the utilisation of the available energy resources. There have also been, and still is, an ongoing transition from conventional power sources, based on fossil fuels, towards renewable energy sources. A lot of the renewable power generation is variable, as to the nature of the renewable power source itself. The increased amount of renewable power production in the system has resulted in two challenges for the system operators when it comes to monitoring and control of the power system. It is difficult to predict the available power from renewable power sources ahead of time, and it demands more complicated system models. Power supply varies a lot (the wind varies in a matter of seconds, for instance), and the power

system must be able to handle such variations, making flexibility more important. Power production from renewable energy sources depends on the availability of the renewable energy. This means that the power production may be situated further away from the customer. Also, a more international power marked, means that more power is sent over large interconnections.

A new monitoring and control scheme is needed, to handle these changes in the power system. The system operator must be prepared to handle large fluctuations in the power generation and have enough power reserves to handle loss of generations or important transmission lines. Since the system can be subjected to fast changes, it is crucial to the system operator that he/she knows about in near-real-time. The change itself may not cause instability in the system, so the system operator also needs to check how the system response if subjected to a potential disturbance. To do this, both model and measurement based stability assessment methods are needed: The measurement based methods, to give regularly measurements, and the model based methods to simulate potential changes in the system.

1.2   Scope of Work

This master thesis will explore the possibility of combining model based methods (based on Supervisory Control and Data Acquisition (SCADA) systems and State Estimation (SE)) and measurement based methods (based on local measurements from PMUs) for on-line voltage stability assessment. Two already existing assessment methods have been implemented and used as the basis for this work. This report does not attempt to bring anything new into the field of voltage stability assessment regarding the theoretical background and implementation. Strengths and weaknesses of the methods chosen compared to other methods will not be discussed, as this is covered thoroughly in other works [11] [8]. The focus will be on how measurement and model based assessment methods may be combined, and how they may complement each other, to improve on-line voltage stability assessment.

The main questions to be answered can be summarised in the following points:

- In what way can the combination of the two methods improve system security (and stability)?

- Compare the results from the continuation power flow and SZ-I. Can the information from the SZ-I be used to improve the results from CPF, and vice versa?

- How well can the proposed method track the maximum loadability?

- How does locally applied voltage control affect the system stability/security?

These questions will be thoroughly treated in the discussion and the conclusion.

1.3 Objectives

The objectives of this master thesis can be split into two parts. First, sufficient ground-work had to be laid, to understand the problem at hand fully, and to obtain the necessary tools to investigate it. The first part can be summed into two points:

1. Literature review on the stability phenomena and security, and on the stability assessment methods

2. Acquire sufficient knowledge about software and conduct the implementation of the methods

This was, in great part, done during the work with the specialisation project but have been further refined during the spring. The second part, and also the main part of this report, includes further implementation and validation of the two assessment methods used, and simulations of an adequate test system and case study:

1. Make a well-suited test case in PSS/E with load variations and contingencies

2. Implement the two methods with simulation results from PSS/E, using MAT-LAB/Python

3. Make a graphical representation that combines the results from the two assessment methods

4. Implement Primary Voltage Control at Bus 1

1.4 Thesis Outline

Chapter 2 will lay the groundwork for understanding the voltage stability problem, different ways of monitoring and assessment methods of stability and security in the power system. The two methods that will be implemented in the case study will be presented in detail.

In Chapter 3 a new on-line assessment scheme, combining model and measurement bases indicators, is proposed. A lot of the work with this master thesis included implementing the methods and running a case study suitable to study them, and this will be explained in detail in Chapter 3.

A case study, where a system goes through two consecutive contingencies and eventually collapses, will be presented in Chapter 4. The proposed method from Chapter 3 will be tested on the case study.

The results from the case study will be discussed in detail in Chapter 5, before a conclusion based on the findings will be given in Chapter 6, to answer the questions put forward in the introduction.

Suggestions for further work will be given in Chapter 7.

1.5 In Relation to the Specialisation Project

The specialisation project presented a literature review on voltage stability and security assessment. A case study was also conducted, where both measurement based and model based on-line stability assessment were implemented and tested for a contingency. The main goal of the specialisation project was to gain more knowledge within the topic of on-line stability assessment and to understand the two different approaches.

Some of the theory from the literature review from the specialisation project [12], that is still found relevant will be included in this master thesis.

The following chapters have been included in their original form: *2.1 - 2.2* (except for *2.2.3*, where some additions have been made), *2.6, 2.7.3, 2.7.5-2.7.7*.

The following chapters have been rewritten: *2.3-2.4, 2.7.4*. They may still bear resemblance to the original chapters but have been changed to include some things that were not included before, or to put emphasis on important parts.

1.6 Clarification of Terms Often Used

Some words that will be used frequently in this report are:

- Stability

- Voltage stability

- Security

- Voltage security

- Security Assessment

- Contingency

Whenever the term stability is used in this report (except for in 2.1), this refers to voltage stability. The same goes for security.

Stability and *security* might seem to be used interchangeably in this report. Therefore it is in order to make the differentiation clear to the reader. *Voltage stability* is the system's ability to maintain voltage. *Voltage security* is the system's ability to operate stable, during normal operation and to *remain* stable when subjected to a *contingency* [13]. The power system security includes the system's robustness to a possible disturbance, i.e., the risk of system disruption [14]. Unplanned outages in the system may happen. Therefore it is necessary also to consider the system security when assessing the system stability in the system. A thorough presentation of both voltage stability and power system security will be given in Chapter 2.

Security assessment includes checking whether the system is stable at its current operating point and whether it is secure, i.e. stable after a disturbance.

2 | Theory

2.1 Power System Stability: An Overview

According to the CIGRÉ task force definition [1] power system stability is defined as

> *"Power system stability is the ability of an electric power system, for a given initial operating condition, to regain a state of operating equilibrium after being subjected to a physical disturbance, with most system variables bounded so that practically the entire system remains intact."*

A thorough presentation of power system stability is given in [7], and some of the fundamental basis will be presented here. Power system stability is in practice, one single problem, but the complexity of instability makes it difficult to solve it as such. Simplifications must be done for every particular type of stability problem, using the appropriate degree of detailed system and analytic model. Stability analysis includes finding the *key factors* causing instability, and the measures to ensure *stable operation* of power systems. Three quantities are important in the operation of power systems stability:

- nodal voltage angles, δ

- frequency, f

- nodal voltage magnitudes, V

On the basis of these three quantities, power system stability is divided into rotor angle stability, frequency stability and voltage stability, presented in Figure 2.1. Rotor angle stability and voltage stability can be further split into small disturbance stability and transient stability. Power systems are nonlinear, and the stability of the system is not only affected by the size of a disturbance, but also the *initial state* of the system at the time it occurs.
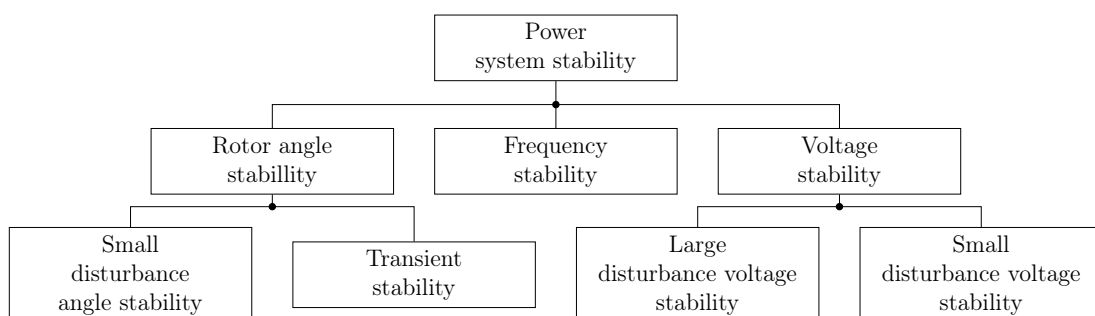
Figure 2.1: Power system stability classification [1]

Rotor angle stability is defined as the ability of the synchronous machines, in an interconnected system, to remain in synchronism under both normal operating condition and after a disturbance. Rotor angle stability is determined by the synchronous machine's ability to maintain or restore equilibrium between electromagnetic torque and mechanical torque.

Frequency stability is defined as the system's ability to stay within the range of the nominal frequency. The frequency in the system is an indication of the power balance in the system. Frequency stability is determined by the system's ability to restore the balance between the power generated and consumed, with a minimum of a load being lost.

Voltage stability is the ability of a system to maintain steady state voltage in normal operation and after both small and large disturbances. A further presentation of voltage stability will be given in the next section.

2.2   Voltage Stability

The CIGRÉ task force have divided voltage stability into four categories; the two first include the size of the disturbance [15]

- *Large-disturbance voltage stability* refers to the system's ability to *maintain* steady voltages after a large disturbance (loss of generation, contingencies, etc.). This is determined by system and load characteristics, controls and protection. The period of study varies from a few seconds, up to several minutes.

- *Small-disturbance voltage stability* refers to the system's ability to maintain steady voltages when subjected to *small* changes, for instance, an incremental increase in the load. Small-disturbance voltage stability is determined by system and load characteristics and system controls.

The two other categories are separated according to the type of system dynamics of interest, and the associated *time frame*

- *Short-term voltage stability* consist of the study of fast acting load components like induction motors, electronically controlled loads and HVDC converters. The analysis period lasts up to several seconds and requires a solution of appropriate differential equations.

- *Long-term voltage stability* consist of equipment with slow acting dynamics, such as tap-changing transformers, thermostatically controlled loads and generator current limiters. The time frame of study is up to several minutes. Long-term simulations can be applied to study system dynamics performance.

To look at it from another point of view, instead, voltage *instability* is defined in [16] as

> "*Voltage instability stems from the attempt of load dynamics to restore power consumption beyond the capability of the combined transmission and generation system.*"

Voltage instability often appears as progressive fall or rise of voltages at some of the buses in the power system. Loads are the *main driving force* for power system instability, but transmission and generation systems also play a significant role. Voltage instability can ultimately lead to a *voltage collapse.* A voltage collapse is defined as a sequence of events that accompanies voltage instability, leading to a blackout or abnormally low voltages in a significant part of the power system [1]. It can be avoided as long as the maximum voltage drop is not exceeded, and as long as active and reactive power margins are large enough for each composite load in each area.

2.2.1 Driving Forces for Voltage Instability

A thorough overview of all aspects related to modelling of power system components, affecting the voltage stability, is given in [16]. Power system component characteristics that affect voltage stability are mainly:

- **Reactive power capacity of generators:** The synchronous generators are the primary source of reactive power support to the system. Characteristics of synchronous generators and the limitations they hold are of great importance when it comes to voltage stability. The amount of reactive power that the synchronous generator can supply are limited by the maximum field current rating, armature heating limit and the maximum turbine power rating. The overexcitation limiter (OXL) protects the field windings of a synchronous machine from overheating caused by too high field currents. The cooling conditions affect how large currents that can be allowed. The synchronous generator will continue to supply reactive power to the grid until maximum field current is reached. In newer systems, the OXL operate together with the automatic voltage regulator (AVR), to control the voltage at the generator terminal. When the field current is the limiting factor, the reactive power production becomes voltage dependent. Armature current limiters, though less common, protects the armature windings from overheating. The armature current limit is upheld by reducing the reactive power output of the machine, by reducing the voltage reference set point of the AVR. Power output, can in some cases be reduced.

- **Maximum power transfer capacity of transmission lines:** The transfer capacity is determined by the thermal limitations or due to stability concerns. The maximum power delivered by the grid can be identified, using PV curves, which will be discussed in 2.2.3.

- **Loads:** Loads are, as already mentioned, often the main driving force for voltage instability. Different types loads affect the system stability differently during a disturbance. Loads are modelled using either static or dynamic load models. *Online load tap changing (OLTC) transformers* is another important type of load. During the recovery process, OLTC will attempt to keep the voltage level at the low voltage side constant, which can lead the system to collapse.

Countermeasures against voltage instability that can be applied will be discussed, but first load modelling and PV and VQ curves will be presented in detail.

2.2.2 Load Modelling

In steady state, the power consumption of a load is determined by the voltage and the frequency at the busbar [7]. $P(V, f)$ and $Q(V, f)$ are the *static load characteristics*. In European power systems, the frequency is nearly constant to 50 Hz at steady state, $P(V)$ and $Q(V)$ are the *voltage characteristics* when the frequency is assumed to be constant. The voltage sensitivities, k_{PV}, and k_{QV}, shows the relationship between change in active power P related to the change in the voltage V, and the same for reactive power Q, for a given operating point.

$$k_{PV} = \frac{\Delta P/P_0}{\Delta V/V_0} \tag{2.1}$$

$$k_{PV} = \frac{\Delta Q/Q_0}{\Delta V/V_0} \tag{2.2}$$

V_0, P_0 and Q_0 are the voltage, active power and reactive power at the initial operating point. A load is stiff if its voltage sensitivities are small, and ideally stiff if they are equal to zero. The active and reactive load dependency differ for different types of loads and thus need to be represented by different mathematical models. All power system analysis programs require such a model. A simple type of load model assumes:

- a constant power demand (P)

- a constant current demand (I)

- a constant impedance demand (Z)

At constant power demand, the power demand is invariant to the changes in the busbar voltage, meaning $k_{PV} = k_{QV} = 0$. This type of load is often used in load flow analyses. For dynamic simulations, the change in load with respect to the change of busbar voltage will be more complex, demanding a mathematical model that takes this into account. A constant current load gives a power demand that will change linearly with the power demand (Ohm's law), $k_{PV} = k_{QV} = 1$. The power in a constant impedance load, will change proportionally with the voltage, $k_{PV} = k_{QV} = 2$. If information about the load composition is missing, real power can be represented by a constant current load and the reactive power can be represented by a constant impedance load, in an exponential load model:

$$P = P_0 \left(\frac{V}{V_0}\right)^{n_p} ; Q = Q_0 \left(\frac{V}{V}\right)^{n_q} \tag{2.3}$$

where $n_p = k_{PV}$ and $n_q = k_{QV}$.

A more general characteristic can be obtained by combining all three characteristics in a ZIP-model, that consists of a sum of constant impedance (Z), constant current (I) and constant power (P).

$$P = P_0 \left[a_1 \left(\frac{V}{V_0}\right)^2 + a_2 \left(\frac{V}{V_0}\right) + a_3\right] \tag{2.4}$$

$$Q = Q_0 \left[a_4 \left(\frac{V}{V_0} \right)^2 + a_5 \left(\frac{V}{V_0} \right) + a_6 \right] \tag{2.5}$$

where a_1 to a_6 and the power factor are the coefficients of the model, and where $a_1+a_2+a_3=1$ and $a_4+a_5+a_6=1$.

The amount of power consumed depends on the voltage characteristics of the load. If the voltage characteristic is constant, the load is purely static. If the voltage characteristic is time dependent, it is dynamic. Load restoration is the process of which load dynamics and control mechanisms restore the load power, at least to some degree.

On-line load tap changers (OLTCs) are slow acting, discrete devices, that changes the transformer tap, one step at a time. The minimum time delay denoted as the mechanical time delay, T_m, is 5 seconds. An additional time delay is often added to avoid unnecessary tap movements, resulting in wear on equipment. The time delay is either constant or variable. For variable time delays, inverse-time characteristics are often used, so that the time-delay becomes shorter for larger voltage errors. The OLTC works within a limited regulation range, with lower limits from 0.85-0.90 pu up to 1.10-1.15 pu upper limit. The size of every tap step is in the range of 0.5%-1.5%. The OLTC lead to load restoration indirectly, by restoring the voltage on the secondary side (distribution side), close to the reference value V_0.

2.2.3 PV and VQ Curves

PV curves show how the power system changes (i.e. the bus voltage changes) as a *function* of the load. PV curves play an important role when it comes to explaining and understanding voltage stability (and instability). PV curves are also called *nose curves*, as the "nose point" of the curve indicates the maximum power transferable by the system to the load. If the load exceeds the "nose point", or the *critical point*, the system can no longer supply the load demand, leading to a voltage collapse.

This can be explained using a simple two bus system, with one generator and one load. The load is fed by a voltage source, $\vec{E} = E\angle 0°$, through a transmission line with impedance Z. Assuming transmission resistance R=0, the resulting voltage at the load bus can be expressed as $\vec{V} = \vec{E} - jX\vec{I}$ and the apparent power consumed by the load can be expressed as:

$$\begin{aligned} S = P + jQ = \vec{V}\vec{I}^* = \vec{V}\frac{\vec{E} - \vec{V}}{-jX} \\ = \frac{j}{X}\left(EV\cos\delta + jEV\sin\delta - V^2 \right) \end{aligned} \tag{2.6}$$

Resulting in $P = -\frac{EV}{X}\sin\delta$ and $Q = -\frac{V^2}{X} + \frac{EV}{X}\cos\delta$. Using the trigonometric identity, $\sin^2\delta + \cos^2\delta = 1$, (2.6) can be reformulated [16] to:

$$v^4 + v^2\left(2q - 1\right) + p^2 + q^2 = 0 \tag{2.7}$$

where $v = \frac{V}{E}$, $p = \frac{PX}{E^2}$ and $q = \frac{QX}{E^2}$, are the normalised quantities. (2.7) forms quadratic equation of the voltage v^2. (2.7) can be solved as:

$$v = \sqrt{\frac{1}{2} - q \pm \sqrt{\frac{1}{4} - p^2 - q}} \qquad (2.8)$$

For the solution of the voltage, v, be bear physical meaning, the following criteria must be satisfied:

$$\frac{1}{4} - p^2 - q \geq 0 \qquad (2.9)$$

The relationship between active and apparent power load, i.e. the *power factor* ($cos\phi = S/P$), influence the shape of the PV curve. There are two possible values for the voltage at a given power load. The upper voltage, provide a resulting lower load current and the lower voltage results in higher load current. Both solutions are *valid* as voltage level concerns, even though the low voltage solution might trigger low voltage protection, but only the upper solution is *stable*. Constant power factor leads to the relationship $Q = Ptan\phi$, between active and reactive power. At maximum loadablity there is only one solution for voltage, i.e., (2.9) equals to zero. Inserting for $q_{max} = p_{max}tan\phi$ gives:

$$\frac{1}{4} - p_{max}^2 - p_{max}tan\phi = 0 \qquad (2.10)$$

(2.10) can be reformulated to:

$$p_{max} = \frac{1}{2}\left(\frac{1 - sin\phi}{cos\phi}\right) \qquad (2.11)$$

High compensation, i.e. small values of $tan\phi$, leads to a higher possible maximum power. The voltage, at which maximum power occurs, is also increased, see Figure 2.2. It might result in voltage levels that are close to the nominal voltage at the point of maximum power. *Over-compensation* happens for negative values of $tan\phi$, i.e. leading power factor. Leading power factor means that higher active power consumption results in more reactive power production at the same time. This result in an increase in voltage until the maximum power limit has been reached.
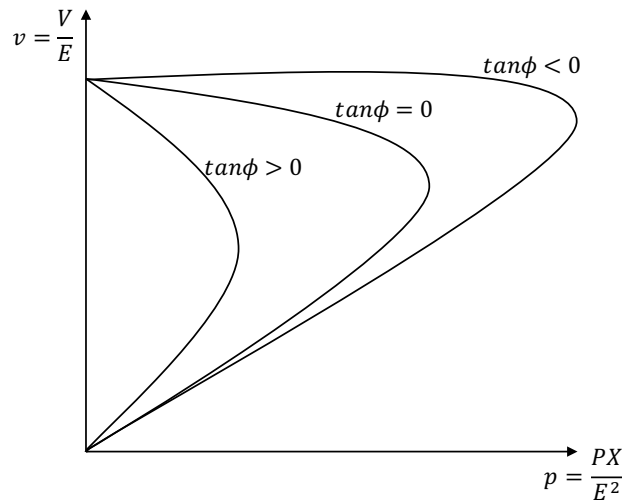
Figure 2.2: v as a function of p for varying power factors

VQ curves provide the relationship between reactive power and voltage for a *constant* active power production or constant power factor. VQ curves can be used to determine how much shunt compensation needed to *restore* or *obtain* the desired voltage level.

2.2.4 Countermeasures Against Voltage Collapse

Countermeasures against voltage instability can be taken in each of the following stages of planning and operation:

- the planning of the power system

- the planning of the system protection design

- the operational planning

- the real-time operation of the power system, monitoring and control

In the planning stage, the reliability criteria must be satisfied for all types of N-1 contingencies. An overview of which of the steps each countermeasure is taken and time scale of response, is presented in [17], and also discussed in [7] and [16]. Countermeasures against voltage collapse include

- **Reactive power compensation switching:** Emergency back-up of reactive power reserves, which are not switched in during normal operation, can be applied as voltage support. The most common types of reactive power support are generators, synchronous condensers and Static VAR Compensators (SVCs). For faster support, they can be connected to the network prior to the disturbance, with sufficient margins. SVCs can maintain the regulated voltage *close* to its set-point, and act almost instantaneous. The range of SVCs are limited, and slower acting devices should be switched in, to *maximise* the availability of the SVCs. Thyristor controlled capacitors are operated through under-voltage relays and can be mechanically switched in fast enough to stabilise a short-term, unstable system. Alternatively, shunt reactors in operation can be tripped, with the same result.

- **Fast start-up of backup generation:** When growing power imbalance appears, fast start-up of hydro or gas turbines might be initiated.

- **Emergency increase of reactive power production from generators:** It is best if the reactive power production happens in the area where the voltage is low. If the generators operate at their capability limit, active power production can be reduced, to help increase the reactive power production. The reduction in power production results in active power imbalance, which must be covered by imported power from other areas, if possible.

- **Blocking OLTC operation:** If the active power demand in the area can not be reduced, reactive power demand can be reduced *indirectly* by bringing back the tap position to predetermined position, to reduce the voltage level on the distribution side.

- **Undervoltage load shedding:** Load shedding is the ultimate countermeasure if none of the countermeasures mentioned above is sufficient. Fast, automatic load shedding set to react when the threshold value of the voltage is reached. Threshold values should be chosen so that this happens only in extreme cases, i.e. for N-2 or N-3 contingencies.

The threshold values for blocking OLTC operations and for undervoltage load shedding fund through off-line analysis. The result from an off-line analysis, will differ from the actual system conditions. Setting the right threshold value is important. If set too low, it can lead to a voltage collapse, and if set too high, it can result in unnecessary voltage reductions and load shedding.

2.3 Power System Security

2.3.1 Defining Power System Security

Security is defined as the freedom from *all* risk and danger. This definition of security is not applicable when referring to the power system. Due to its sheer size and complexity, in addition to its vulnerability to external forces, it can never be a hundred percent secure [14]. *Power system security* is defined as the ability to survive a contingency without violating the system constraints [1]. A *contingency* is defined as an *unplanned* outage of one or more primary system component. Whenever a power system is subjected to a sudden change or contingency, it is desirable that the power system settles such that all system constraints (bus voltages, line flow limits, etc.) are within given limits.

Power system constraints can be divided into *load demand* constraints and *operating* constraints [16]. Load demand constraints take the form of equality constraints and state whether the load demand in the system is met or not. The total power production must be *equal* to the total power consumption and transmission losses in the system to fulfil the load constraints. The operation constraints are given by inequalities constraints and specify the maximum and/or minimum operating limits that the system components can endure. These includes allowed voltage range at the buses, maximum allowed power transfer through the lines, line currents, etc., all of which may overload and harm the system components. Any violation of the security constraints may drive the power system towards the stability limit.

2.3.2 Power System Operating States

There are five different *defined* operating states of the power system [2]. The different states and the transition between them, are presented in Figure 2.3. Whether the load constraints, denoted by D, and the operating constraints, denoted by O, are met or not, is indicated for each of the states in the figure.

When the system operates in *normal* state, both the load demand constraints and the operating constraints are met. A system is *secure* if it remains stable after a contingency, i.e. the system has enough reserve margins to withstand any plausible N-1 contingency. It is desirable that the power system remains in a *normal and secure* operating state at all times, but due to changes in loads, contingencies, etc., this is not the case. If anything happens to cause the system to move to another operating state, control actions must

be taken, to bring the system back to the normal and secure state. The green arrows in the figure indicate the control actions. Any transition to another state, caused by a disturbance in the power system, is indicated by a red arrow.
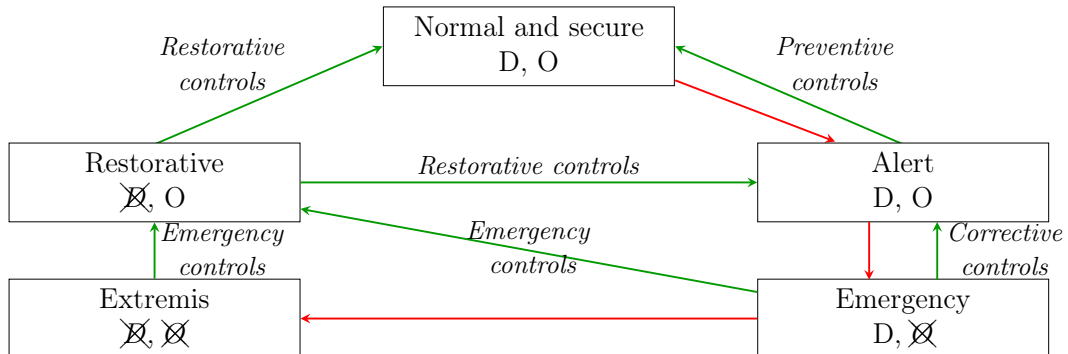
Figure 2.3: Power system operating states [2]

If a system is in normal and *insecure* state, all constraints are met, but the reserve margins are not large enough to guarantee that the system will remain in the normal state after a severe disturbance. This state is also called the *alert state*. *Preventive controls* are controls that can be applied *beforehand* of a potential contingency, and includes restoring adequate reserve margins, generation shifting, tie-line rescheduling, etc., so that the system becomes secure again. It is not profitable to protect the system from *all possible* contingencies. The economic costs of preventing the system from becoming unstable must be weighed against the likelihood of it occurring, and the total cost of the consequences if it does.

If preventive measures are not taken, and a contingency occurs, the system moves to the emergency state. In the emergency state, the power system will continue to supply the loads at the expense of violating the operating constraints. Depending on the severity of the disturbance, *corrective controls* might bring the system back to the alert state or *emergency controls* might bring the system to the *restorative state*.

If control actions are not taken, or not taken *fast enough*, or if the contingency that occurs in the alert state is severe, the system goes into the extremis state. In this state, both the operating constraints and the load demand constraints are violated. This may lead to tripping of generators, due to loss of system synchronism and in the worst case, total or partly blackout of the system.

To bring the system from the extremis state to the *restorative state*, the system operator sets in emergency control actions, that includes reconnecting all facilities and restore the system loads. In the restorative state, operation constraints are met, but the load demand constraints are not. Restorative control actions attempt to restore all lost loads and reconnect the system, and re-synchronisation of the whole system. Depending on the current situation in the system, the system transits to either normal and secure state, or to normal and insecure state.

2.3.3 Power System Security Assessment

Power system security assessment is, as the name imply, a way to assess the power system to determine the current power system operating state. Power system assessment can be divided into three levels [16]:

- **Security monitoring:** Check whether or not the system state satisfies the operating constraints and the load demand constraints, i.e. *whether the system in normal state or not.*

- **Security analysis**: Check the system's ability to *endure* a disturbance, i.e. *whether the system is secure or insecure.* The system is only checked for the most plausible contingencies, loss of one component (N-1) or multiple contingencies that are likely to occur at the same time.

- **Security margin determination**: Check how far the current operating point is from the stability limit, either the distance to *post-contingency loadability limit* or to the *secure operation limit.* This information can be used to ensure an adequate security margin.

Security analysis and security margin determination are more computationally demanding, as they rely on not only system measurements, but also system models to simulate the effect of contingencies that have not yet happened.

The security assessment can be classified into two, based on which analysis method that is used. *Static Security Assessment* (SSA) is used to assess the pre-contingency or the post-contingency operation state of the network. In the pre-contingency operation state, SSA is used to determine the available capacity of the transmission links and to identify network congestion. For the post-contingency operation state, SSA is used to verify that the bus voltages and line power flow are within limits after a disturbance. SSA assumes that the transition between the pre- and post-contingency operating states happen without any part of the system experiencing instability phenomena.

Dynamic Security Assessment (DSA) is used to evaluate the stability and the quality of the process *between* the pre- and post-contingency states. Because the transition is studied, both the dynamics of the system and protection schemes come into play. DSA aims to ensure that the system returns to a stable state after a contingency and that the transients, caused by it, will be well damped, of small amplitude and with little impact on the quality of service [3].

2.4   On-Line DSA System

2.4.1   Moving Towards On-Line DSA

Both SSA and DSA (presented in 2.3.3), have in the past been conducted off-line, doing time-domain stability analyses with forecast data. Often, these were carried out in the planning stage, when building a new transmission line for example. The requirements for security assessment have increased due to liberalisation, more renewable energy sources, etc., and off-line assessment is no longer sufficient to ensure a secure operation of the power system.

In *on-line* DSA, a snapshot of the *actual* system state is used as input, assessing the security in near-real-time. On-line DSA almost works like a radar. It sweeps the system and gives the operator an indication of the current system state, and warns him or her if the system moves to the alert state. Working with sufficient speed, on-line DSA hopefully makes it possible to trigger automatic control or gives the operator enough time to set in manual control.

A basic on-line DSA framework includes essentially two steps [18]. The first step is to do a screening of the system, to determine which of the contingencies to study in more detail. The contingencies that are found to be *"sufficiently"* stable are not studied further. A selection of contingencies that are considered only *"marginally"* stable are examined in greater detail, using time-domain analysis in step two. In on-line DSA, the computation time is a significant constraining factor, as well as the interpretation and the quantification of the results. Figure 2.4 gives an overview of the components of an on-line DSA system according to the CIGRE Report No. 325.
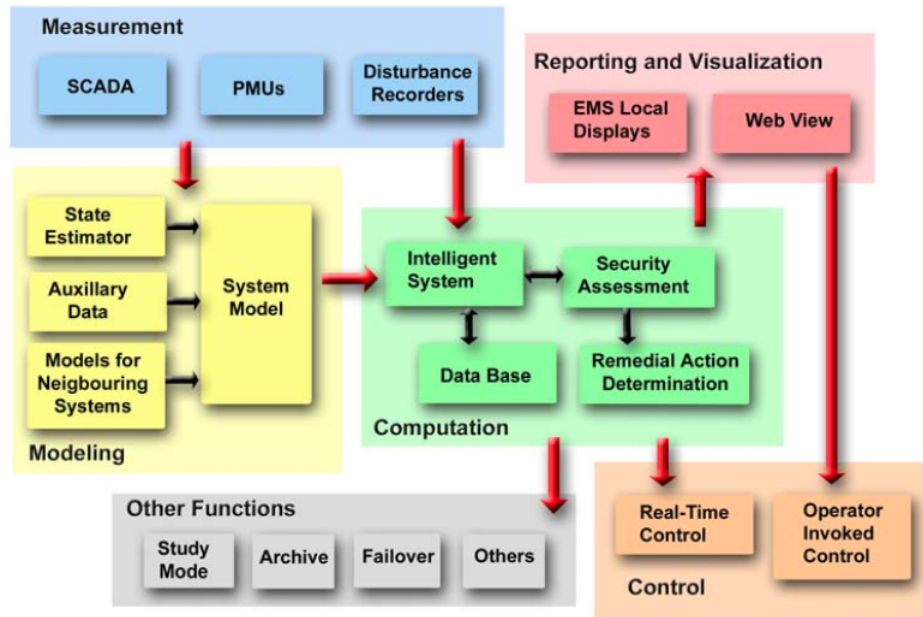
Figure 2.4: The components of an on-line DSA system [3]

2.4.2 Measurements

A prerequisite for security assessment systems is to receive measurements that are accurate enough and comes frequently enough. Today, these are provided by the Supervisory Control and Data Acquisition (SCADA) system and the Phasor Measurement Units (PMUs).

"For on-line DSA purposes, useful measurements include,

- Active power of most power lines, power transformers and generators
- Reactive power of most power transformers, shunt reactors, shunt capacitors and generators
- Voltage of most substations
- Frequency measured at a few locations of the grid
- Status of most network switched related to power lines, power transformers and generators
- Transformer tap positions." [3]

2.4.3 SCADA Systems

Conventional monitoring systems are based on the measurements provided by the SCADA system. The measurements are conducted at substations in the power system and sent from the Remote Terminal Units (RTU) and the Intelligent Electronic Devices (IED) to the SCADA system. The SCADA system provides the measurements to the Energy Manager System (EMS), that contains planning and analytic functions. These require that the *system state*, i.e. the complex phasor voltages ($V_i \angle \delta_i$) at *all* buses, is known. If the system state, network model and parameters are known, the operating condition of the system can be obtained for further analysis in the EMS.

The accuracy of the measurements from the SCADA system is subjected to uncertainty. Malfunction of measurement devices, communication errors, erroneous system model or unexpected changes in the system (switching, loss of line, etc.), can lead to measurement imprecision or loss.

The state estimator (SE) provides the EMS with the *system state*. The SE estimates the system state that matches best with the available measurements while minimising the measurement error. The complete SE problem formulation and the solution technique can be found in [19].

The SCADA system does not conventionally measure voltage phasors, so these must also be estimated by the SE. One assumes that all measurements are synchronised, but that is not the case. The time that it takes to receive measurements from various locations in the system varies, and there is no way to ensure that they are referred to the same time stamp. Since the measurements are not completely synchronised, this can sometimes lead to contradictory measurements.

2.4.4 PMUs and WAMS
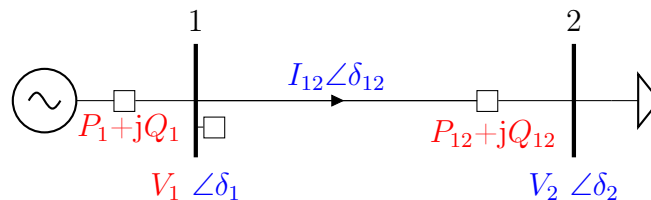
Figure 2.5: Measurements in the system (red: SCADA systems, blue: PMUs)

Figure 2.5 shows a simple two-bus system, with both SCADA system measurements and measurements provided by the Phasor Measurement Unit (PMU), indicated. The most prominent feature of PMU is the additional measurements of *phase angle*. PMUs were first introduced in the early 80s, and have since then become a mature technology with many applications that are still under development today [4]. A PMU is a digital device that provides synchronised voltage and current phasor measurements, referred to as synchrophasors [20]. Whereas the SE only provides an *estimate* of the power system state, PMUs provide real-time measurements of some buses in the system. PMUs can be used to verify and tune the results obtained by the SE, to provide a better estimate of the system state.

PMUs are placed at substations in the network and measure the frequency of the alternating voltage and current. The input data to the PMU are sampled with reference to the Universal Time Coordinated (UTC) time, provided by the Global Positioning System (GPS) satellites. The phasor angle of the measured voltage and current is the *angular difference* between the peak value of the sinusoid and the reference time t=0 (see Figure 2.6), where the reference time corresponds to the time-tag. Data from several PMUs are collected by a special-purpose computer, Phasor Data Concentrator (PDC), and combined to create a system-wide measurement set [21].

The resulting phasor measurements can be reported at about the same rate as the fundamental frequency. With a fundamental frequency of 50 Hz, that means that new data is aggregated 50 times per second, i.e. new measurements from the system are collected every 20 ms.

Since PMUs measure both voltage and line currents at a substation, PMUs are not needed at all buses. Given that transmission line parameters are known, in addition to the line currents, the voltage at neighbouring buses can be computed. To obtain full observability of the system, PMUs need to be placed at approximately one-third of the buses in the system.
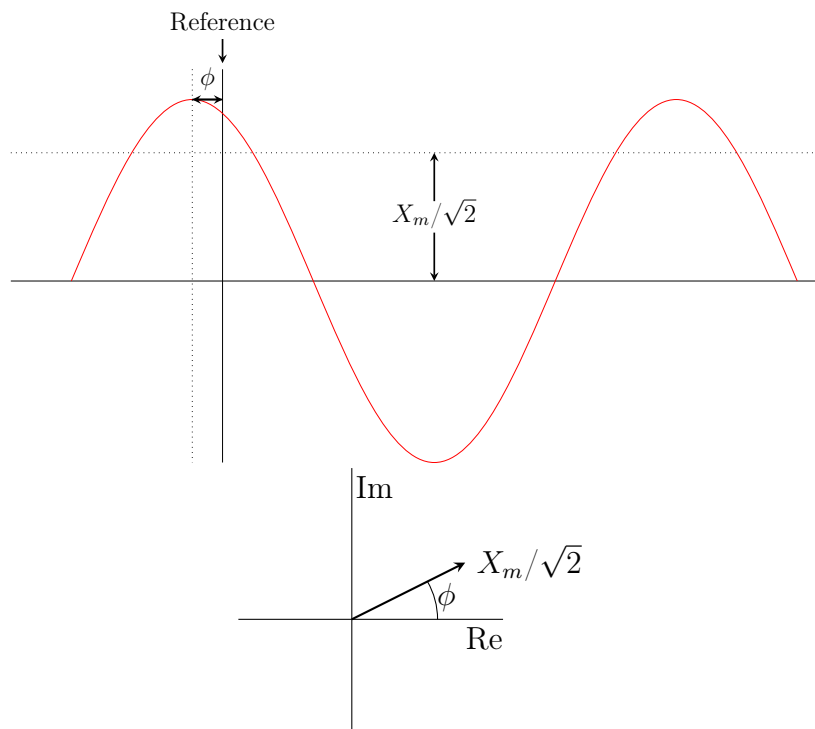
Figure 2.6: Sinusoidal representation and the corresponding phasor representation [4]

2.4.5 Instability Monitoring Based on Local Measurements from PMUs

Local relays are used to determine if the current loading, connected at the substation, is causing too much strain on the system [8]. Based on local measurements of voltage and current provided by the PMU, it is possible to estimate the strength of the transmission system. The strength of the transmission system determines if the transmission capacity is sufficient to sustain the load. This approach does not need off-line simulation tools, experience or load models, and relies solely on the measurements. Therefore, it is possible to conduct a fast and exact assessment of the system. As can be seen in Figure 2.7, it is in the corrective (or emergency) line of defence that this type of PMU technology can increase system monitoring, most significantly [22].
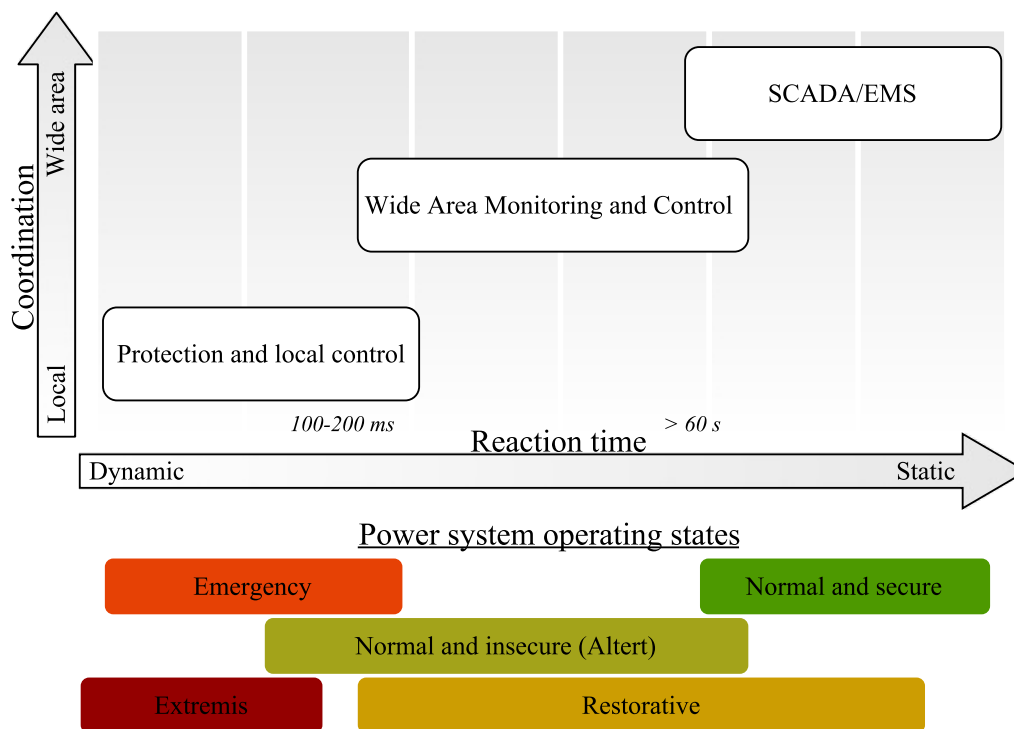
Figure 2.7: Reaction time for protection, monitoring and control equipment, in relation to the coordination for different power system operating states [5]

2.5 Voltage Control

When the operating conditions changes, control actions need to be set in, if the system is to *remain* in a stable operating state (see Figure 2.3). Some of these control actions are automatic, but most of them must be applied manually. Manual control relies, in large, on the experience and ability of the system operator. According to [23], voltage control is best achieved if there is some degree of automation among the reactive control systems.

2.5.1 Voltage Control Hierarchy in Power Systems

In power systems, most system operators have set the limit for voltage to be $\pm$ 10 % of the nominal voltage. In transmission networks, the main objectives of voltage control are to maintain continuous high (and flat) voltage profile, to minimise power system losses and increase the voltage stability margin. In the distribution grid, the main objectives of voltage control are to maintain voltage levels within acceptable limits at customer terminals, minimise local system losses and increase the voltage stability margin in the distribution area.

Voltage control can be divided into three hierarchy levels (see Figure 2.8), classified according to their operating time frame (time constant) and operating geographical range [23]:

- Primary voltage control (component control)

- Secondary voltage control (areal control)

- Tertiary voltage control (power system control and optimisation control)

Primary voltage control is performed by automatic voltage regulators (AVRs) on the generators, OLTC of the transformers, the synchronous condensers and by static VAr compensation [24]. These are automatic voltage controls that set in within milliseconds after changes in the voltage level. The voltage control is applied locally, i.e. at the generator bus, etc.
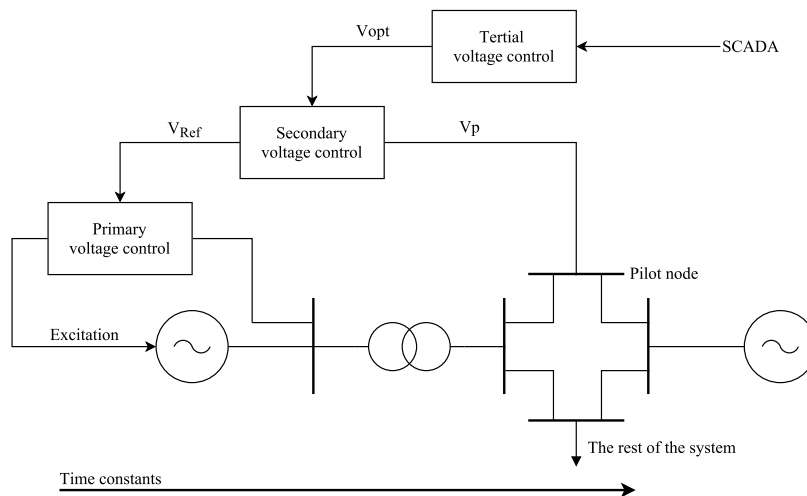
Figure 2.8: Voltage control hierarchy [6]

Secondary voltage control provides voltage support at a regional level, by coordinating the primary controls in the area. The power system can be split into areas that are weakly linked to each other. The secondary voltage control controls the voltage level of a load bus in the area, called a pilot bus or pilot node, to a predetermined level. It is set to act slower than the primary voltage control and operates in the range of seconds to a minute.

Tertiary voltage control is not as widely used as primary and secondary voltage control. It operates every 5 to 15 minutes and utilises an optimal power flow (OPF) program in an off-line environment. OPF is done to minimise transmission losses, maximise reactive

power reserves close to load centre and to increase stability margins. The results can be utilised to reset the set-points of the pilot buses, and MVAr provided by the generators and capacitor/reactor banks. Coordinated switching of capacitor/reactor banks can be performed by both secondary and tertiary voltage control, to keep the voltage level flat, even in heavy loaded situations.

2.5.2 FACTS and FACTS Devices

Traditionally, the main controllers in the power systems (like tap changers on transformers) were mechanical devices, and rather slow. The development of power electronics has led to the development of devices with the same functions, but which are faster and have less technical issues. Power systems equipped with this type of equipment are called Flexible AC Transmission Systems (FACTS), while the power electronics go under the name of *FACTS devices*. FACTS devices are switched in and out by semiconductors, also known as thyristors. Two types of FACTS devices that can be used for voltage control, shunt connected (static VAr compensators (SVCs) and static compensators (STAT-COMs)) and unified power flow controllers (UPFCs). The SVC will be used in the case study and will be given a more thorough introduction.

2.5.3 SVC

SVCs were first introduced in the 1970s. They are based on conventional thyristors, silicon controlled rectifiers, that only have turn-on capability. SVCs are considered as old technology, and the expenses tied to necessary filtering, generally makes other solutions more desirable.
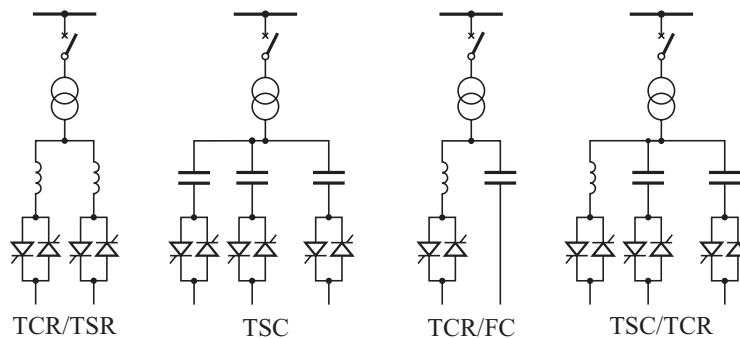
Figure 2.9: Typical configurations of SVCs [7]

Examples of different configurations of SVCs are presented in Figure 2.9. The configurations consist of the following types of SVCs: thyristor-controlled reactor (TCR), thyristor-switched reactor (TSR), thyristor-switched capacitor (TSC) and fixed capacitor (FC).

Smooth control of current is not possible by control of capacitors, due to the long time constant in relation to charging/discharging, so capacitors are either switched in or out. SVCs can be designed to operate in both the capacitive and the inductive area, using thyristor-switched and/or thyristor-controlled shunt elements.

2.6 Continuation Power Flow

There are four elements in the Continuation Power Flow method:

- parametrisation

- predictor

- corrector

- step-length control

These will be explained in detail, but first, some background information and the motivation behind CPF will be presented. Continuation power flow was first proposed by Venkataramana Ajjarapu and Colin Christy in 1992 [25]. The continuation power flow (CPF) method finds a continuum of power flow solutions. From an initial power load, the load is increased, until the *steady state*, voltage stability limit is reached, i.e. the critical point (P_{max}). An attempt to increase the power beyond this point will lead to a voltage collapse. Close to the critical point, the Jacobian matrix of the Newton-Raphson method becomes singular, and the determinant of the inverted Jacobian becomes zero. Solving power flows near the critical point will lead to prone divergence or error.

The CPF method was developed in order avoid that the Jacobian becomes singular. The power flow equations are reformulated to include a *load parameter* and the parameters are locally applied. Figure 2.10 and 2.11 illustrate the CPF method. CPF is also called the predictor-corrector method. The starting point is a known solution, and the CPF method consists of two steps, the predictor step and the corrector step. The predictor-corrector scheme finds the next solution corresponding to the *new* power loading.
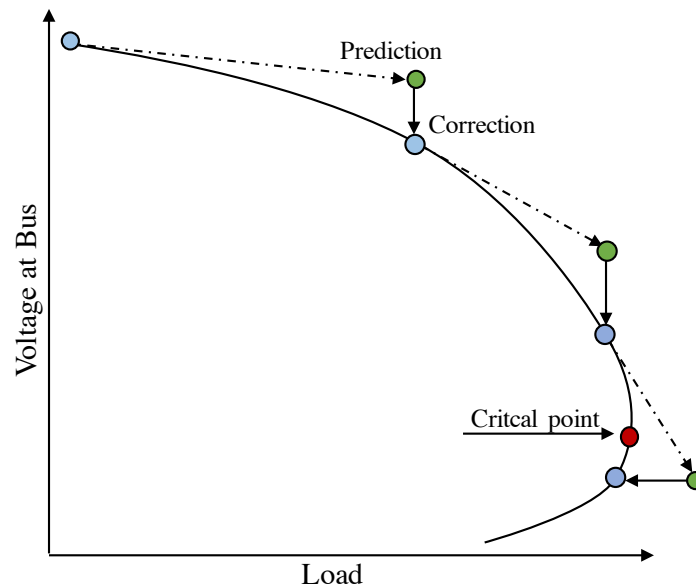
Figure 2.10: The continuation power flow process - the green dots indicate the *predicted* solution and the blue dots the actual solution on the PV curve after the correction step.

2.6.1 Reformulation of Power Flow Equations

The power flow equations used in the ordinary power flow analysis, are reformulated in CPF to include a load parameter, λ:

$$f(x, \lambda) = g(x) - \lambda d \qquad (2.12)$$

where $0 \leq \lambda \leq \lambda_{crit}$. λ equals zero corresponds to the base case power loading, and λ equals λ_{crit} corresponds to the critical point, P_{max}. For a constant power load model, a load parameter, λ, that represents the load increase in direction d is introduced [26]:

$$\Delta P_k = P_{Gk}(\lambda) - P_{Lk}(\lambda) - P_k(\delta, V) \qquad (2.13)$$

where

$$P_{Lk}(\lambda) = P_{Lk}^0 + \lambda d \qquad (2.14)$$

and

$$\Delta Q_k = Q_{Gk}(\lambda) - Q_{Lk}(\lambda) - Q_k(\delta, V) \qquad (2.15)$$

where

$$Q_{Lk}(\lambda) = diag(tan\phi) P_{Lk} = Q_{Lk}^0 + \lambda \cdot diag(tan\phi) d \qquad (2.16)$$

$$tan\phi = \frac{Q_0}{P_0} \qquad (2.17)$$

P_{Lk}^0 and Q_{Lk}^0 are the base case active and reactive power. Initial operating condition are given by the voltage magnitude, voltage angle and power loading at base case:

$$z_i = [x \ \lambda] = [\delta \ V \ \lambda] \qquad (2.18)$$

The CPF process is shown in (2.19). The starting point is at the previous solution, then a predicted solution is found in the predictor step. The corrector step finds the next actual solution on the curve.

$$(x_i, \lambda_i) \xrightarrow{Predictor} (x_{i+1}^p, \lambda_{i+1}^p) \xrightarrow{Corrector} (x_{i+1}, \lambda_{i+1}) \qquad (2.19)$$

2.6.2 Parametrisation

The resulting solution curve, see Figure 2.10, is created by the joining the corrected solutions together. Parametrization is a mathematical way to quantify all the solutions, given (x, λ), on the curve.

The values of (x, λ) can be parametrised in different ways. The simplest way, is using *natural parametrisation* or *physical parametrisation*, where the new loading λ can be found by simply adding the step length, σ, to the previous solution, λ^j.

$$\lambda^{j+1} - \lambda^j - \sigma = 0 \qquad (2.20)$$

The second type of of parametrisation is *arc length parametrisation*, where the step size σ is equal to the 2-norm of the distance between the previous solution and the next solution.

$$\sum_i (x_i - x_i^j)^2 + (\lambda - \lambda^j)^2 - \sigma^2 = 0 \qquad (2.21)$$

The third type of parametrisation, is called *pseudo arc length parametrisation* [27], and uses weighting factors. This is done, in order to constrain the next solution (x, λ) to lie in the hyperplane, that goes through the predicted solution $(x_{i+1}^p, \lambda_{i+1}^p)$ orthogonal to the tangent line from the previous solution (x^j, λ^j).

$$\sum_i^{2(n-I)} (x_i - x_i^j)^2 + (\lambda - \lambda^j)^2 - \sigma^2 = 0 \tag{2.22}$$

2.6.3 Predictor-Step

The predictor-step finds an approximation for the next solution. One way to do this is by using the tangent-method. The tangent-method uses the tangent, t_i, at a given position z_i. Initial position z_i can either be found from an initial load flow at the base load or a previous CPF solution (see Figure 2.11). The predicted solution, z_{i+1}^p is found by multiplying the tangent vector, t_i, with the step length σ, and add this to the current solution, z_i. It is important to note that z_{i+1}^p does not correspond to a physical operating point.

$$z_{i+1}^p = z_i + \sigma t_i \tag{2.23}$$

The first step is to calculate the tangent vector, $\underline{t_i}$. It must be obtained so that:

$$J(z_i) \, \underline{t_i} = 0 \tag{2.24}$$

where

$$t_i = [d\delta \ \ dV \ \ d\lambda]^T \tag{2.25}$$

The Jacobian matrix, is expanded to also include λ:

$$J(z_i) \, t_i = \begin{bmatrix} \frac{\partial \Delta P}{\partial \delta} & \frac{\partial \Delta P}{\partial |V|} & \frac{\partial \Delta P}{\partial \lambda} \\ \frac{\partial \Delta Q}{\partial \delta} & \frac{\partial \Delta Q}{\partial |V|} & \frac{\partial \Delta Q}{\partial \lambda} \end{bmatrix} t_i \tag{2.26}$$

Element k of $\underline{t_i}$ is set to

$$t_k = \begin{cases} 1 & \text{if loading is increasing} \ (+\lambda) \\ -1 & \text{if voltage or loading is decreasing} \ (-V_k \text{ or } -\lambda) \\ 0 & \text{if the } k^{th} \text{ value is kept constant} \end{cases} \tag{2.27}$$

The tangent vector, $\underline{t_i}$, has to be normalised for it to not get a nonzero length.

$$e_k^T \underline{t_i} = t_k = \pm 1 \tag{2.28}$$

e_k^T is a row vector added to the Jacobian matrix. All elements of e_k^T are zero, *except* for the element that corresponds to the kth element of $\underline{t_i}$.

$$\begin{bmatrix} \frac{\partial \Delta P}{\partial \delta} & \frac{\partial \Delta P}{\partial |V|} & \frac{\partial \Delta P}{\partial \lambda} \\ \frac{\partial \Delta Q}{\partial \delta} & \frac{\partial \Delta Q}{\partial |V|} & \frac{\partial \Delta Q}{\partial \lambda} \\ & e_k & \end{bmatrix} \underline{t_i} = \begin{bmatrix} 0 \\ \pm 1 \end{bmatrix} \tag{2.29}$$

2.6.4 Corrector-Step

The next step is to determined *which* element in z_i to keep constant, and which ones to vary, in the corrector-step. Either δ, V or λ is kept constant.

$$\begin{bmatrix} f(z) \\ z_k - \eta \end{bmatrix} = 0, z = \begin{bmatrix} \delta \\ V \\ \lambda \end{bmatrix} \tag{2.30}$$

η is an appropriate value of element k of z. The correct continuation parameter at each step, is done choosing the state variable that has the largest tangent vector component, t.

$$z_k : |t_k| = max\{|t_1|, |t_2|, \cdots, |t_m|\} \tag{2.31}$$

The maximum point of λ is where dλ is zero. As long as dλ is bigger than zero, λ is increased, but once dλ becomes negative, maximum loading point has been bypassed.

2.6.5 Step-Length Control

Even though it is safe to choose a constant small step size, this can in many cases leads to inefficiency. Selecting a step length that is too large, however, can result in considerable imprecision in the predicted step. Ideally, the step length should follow the shape of the curve, i.e. long steps in the flat part of the curve, and shorter steps closer to the tip of the curve. One way, of ensuring that the length is not too big, is setting a σ_{max}. An adaptive step size can also be applied, where a target number of iterations taken at each step is set. If the number of actual iteration steps is smaller than the target number, the next step length can be set to be a little bit larger than the previous step length.
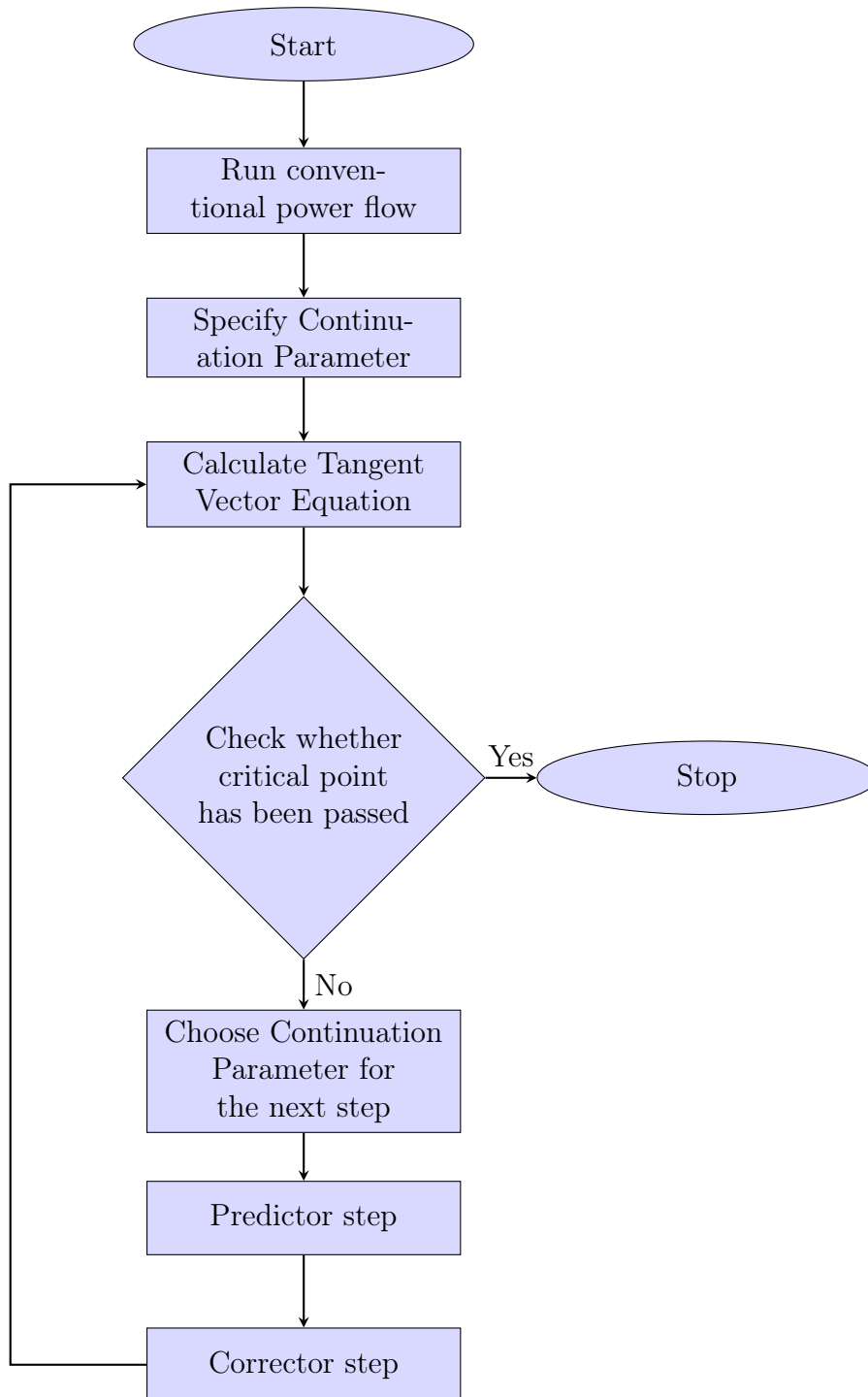
Figure 2.11: Flow chart of continuation power flow algorithm.

2.7 S-Z Sensitivity Indicator (S-ZI)

Doung's PhD thesis introduces the S-Z sensitivity indicator (S-ZI) for on-line voltage stability monitoring of the system. The indicator can be computed directly from the measurements of voltage and current from the PMU placed at the load bus. The method does not require a model of the network and is easy to calculate. The S-ZI can be utilised to estimate a Z_{Th} of the simplified Thevenin equivalent model of the system, that can be used to determine the maximum transfer capability of the system. The following section is mainly based on the content presented in Chapter 3 of [11].

2.7.1 Thevenin Equivalent Network

The circuit diagram in Figure 2.12 is a representation of the power system seen from the load bus. The voltage at the load bus is denoted by $\vec{V}$, and the load is denoted as the impedance Z_L. The rest of the power system is represented by a Thevenin equivalent, with the voltage source, $\vec{E_{Th}}$, and the impedance, $\vec{Z_{Th}}$.
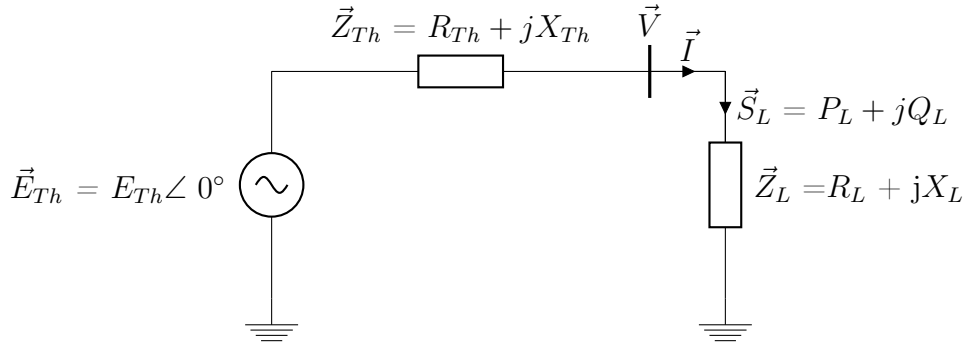
Figure 2.12: Thevenin equivalent network

2.7.2 Maximum Power Transferred by the Grid

The current $\vec{I}^*$ can be calculated from:

$$\frac{P_L + jQ_L}{\vec{V}} = \vec{I}^* = \frac{\vec{E_{Th}} - \vec{V}}{\vec{Z_{Th}}} \tag{2.32}$$

Where the expression to the left is the current seen from the receiving end (with a power transfer of $P_L + jQ_L$ to the load), and the expression to the right seen from the sending end. Reformulating (2.32), gives the following expression for the resulting voltage at the given power transferred:

$$(P_L + jQ_L) \cdot \vec{Z_{Th}} = \vec{V} \left(\vec{E_{Th}} - \vec{V} \right)^* \tag{2.33}$$

where $\vec{V}$ is one solution and $\left(\vec{E_{Th}} - \vec{V} \right)^*$ is another solution for the voltage. At maximum power the two solutions become one, i.e.:

$$\vec{V} = \left(\vec{E_{Th}} - \vec{V}\right)^{*} \qquad (2.34)$$

Any further increase in the load ($dZ_L < 0$), does not yield a solution. (2.34) can be reformulated to:

$$\vec{Z_L} \cdot \vec{I} = \left(\vec{Z_{Th}} \cdot \vec{I}\right)^{*} \qquad (2.35)$$

or simplified even further to:

$$\left|\vec{Z_L}\right| = \left|\vec{Z_{Th}}\right| \qquad (2.36)$$

No assumptions are made about the load characteristics, the value of $\vec{Z_L}$ is based solely on the measurements of the voltage and current at the bus. The system is stable as long as $\vec{Z_L}$ is outside of the circle created by Z_{Th} (see Figure 2.13), or more simply stated, as long as $|\vec{Z_L}| > |\vec{Z_{Th}}|$. The distance from $\vec{Z_L}$ to Z_{Th} determines how close the system is to its maximum power transfer limit. The value of Z_{Th} is not a fixed quantity either and will vary as the network topology, available power generation and demand changes, as well as changes in available VAr resources.
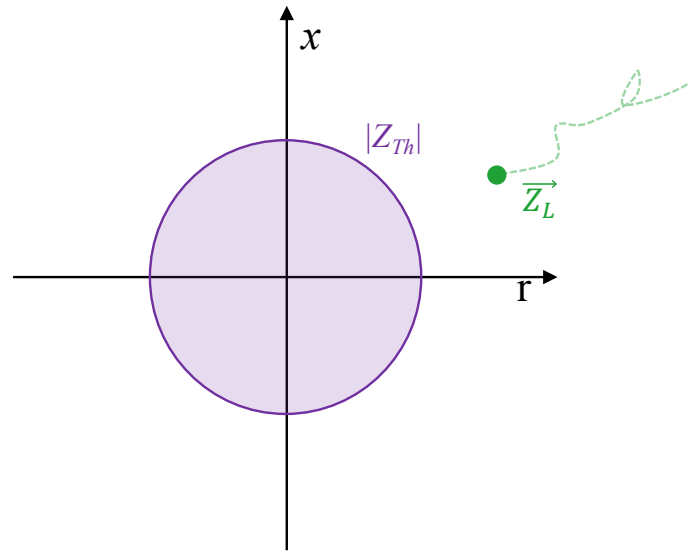
Figure 2.13: Maximum power transfer [8]

Z_{Th} can only be verified when the system reaches the stability limit. At the maximum power transfer, it is known from (2.36) that the Thevenin impedance is *equal* to the load impedance. With a simple two bus system, that only contained one single generator, one load and one line impedance, Z_{Th} could be found more accurately for other operating conditions. The system is only *simplified* to a Thevenin equivalent network, but in practice, it does not capture the actual impedance of the network.

2.7.3 Development of S-ZI

The load current magnitude, I (cf. 2.12), can be found from:

$$I = \left| \frac{\vec{E}_{Th}}{\vec{Z}_{Th} + \vec{Z}_L} \right| = \frac{E_{Th}}{\sqrt{(R_L + R_{Th})^2 + (X_L + X_{Th})^2}} \tag{2.37}$$

The denominator can also be expressed in terms of impedances as:

$$I = \frac{E_{Th}}{\sqrt{Z_{Th}^2 + Z_L^2 + 2(R_L R_{Th} + X_L X_{Th})}} \tag{2.38}$$

Rearranging $R_L R_{Th} + X_L X_{Th}$ to $Z_L Z_{Th}(cos\theta_L cos\theta_{Th} + sin\theta_L sin\theta_{Th})$, and using the trigonometric identity $cosX cosY + sinX sinY = cos(X - Y)$ yields:

$$R_L R_{Th} + X_L X_{Th} = Z_L Z_{Th} \cos \theta \tag{2.39}$$

with the resulting θ, denoting the angle difference between the load impedance Z_L and the Thevenin impedance Z_{Th}. Insert (2.39) into (2.38)

$$I = \frac{E_{Th}}{\sqrt{Z_{Th}^2 + Z_L^2 + Z_L Z_{Th} \cos \theta}} \tag{2.40}$$

The apparent power, S_L, consumed by the load, can be found by inserting (2.40) in the conventional formula:

$$S_L = I^2 Z_L = \frac{E_{Th}^2 Z_L}{Z_{Th}^2 + Z_L^2 + Z_L Z_{Th} \cos \theta} \tag{2.41}$$

$$\frac{dS_L}{dZ_L} = \frac{I^2 (Z_{Th}^2 - Z_L^2)}{Z_L^2 + Z_{Th}^2 + 2Z_L Z_{Th} \cos \theta} \tag{2.42}$$

$\frac{dS_L}{dZ_L} = \zeta$, and will here after be called S-Z sensitivity. Rearranging of (2.42) result in a second order equation, with Z_{Th} as the *unknown* variable.

$$(I^2 - \zeta)Z_{Th}^2 - 2\zeta \cos \theta Z_L Z_{Th} - Z_L^2 (I^2 + \zeta) = 0 \tag{2.43}$$

The phasor measurements provide measurements of the voltage and current with phasors at the buses. Z_L and S_L can be obtained from these data, and dS_L and dZ_L can be calculated using *consecutive* measurements.

To find the angle difference, θ, both the load impedance angle, θ_L, and the Thevenin impedance angle, θ_{Th}, must be found. θ_L can be calculated from the measurements, θ_{Theta} is primarily determined by the impedance of the lines in the area. The X/R ratio of the lines in the area can be used as an approximation of θ_{Th}. The value of $cos\theta$ is assumed constant (assuming constant θ_{Th} and θ_L).

2.7.4   Trajectory: the Impact of the X_{Th}/R_{Th} Ratio

The X_{Th}/R_{Th} ratio of network must be determined before (2.43) can be solved to find Z_{Th}. For a sufficient large value of X_{Th}/R_{Th}, it can be shown that the deviation of Z_{Th} becomes small. Every calculated Thevenin impedance has its own distinctive trajectory (see Figure 2.14).
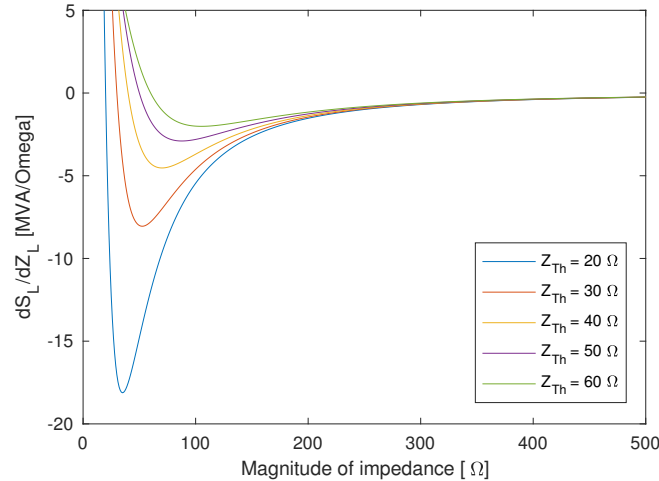
Figure 2.14: Trajectory of S-ZI with different values of Thevenin impedance Z_{Th}

In Figure 2.14, the trajectories for different values of Z_{Th} are plotted. For high values of Z_L, i.e. light loading, the S-Z sensitivities are similar for all values of Z_{Th}. For heavier loading, there are large differences in the resulting S-ZI. The operating point must lie to the left on the curve (low Z_L) if the X_{Th}/R_{Th} is to be determined accurately.

To check whether X_{Th}/R_{Th} is correct or not, the estimated Z_{Th} can be used to find E_{Th} and dS/dZ can be calculated using (2.42) for different values of the load impedance Z_L. If the correct X_{Th}/R_{Th} is chosen, Z_L and S-ZI coincide with the trajectory drawn by the estimated Z_{Th} (see Figure 2.15).
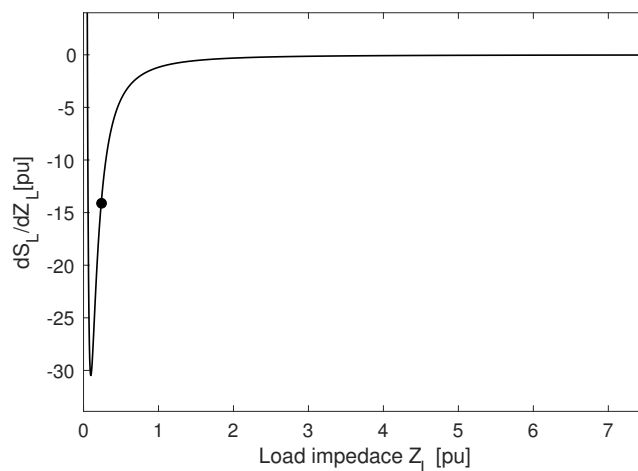
Figure 2.15: Example of trajectory with a good estimation of the X_{Th}/R_{Th} ratio

The maximum power transfer can be found when Z_{Th} has been determined, using (2.11) from Section 2.2.3. The Thevenin voltage source E_{Th} can be found by simply adding the voltage drop across over the transmission line to the voltage magnitude measured at the load bus:

$$E_{Th} = |V + (R_{Th} + jX_{Th}) \cdot I| \tag{2.44}$$

When P_{max} have been found the PV curve can be plotted using (2.8). The resulting PV curve for Figure 2.15 is plotted in Figure 2.16. The current operating point is indicated by the black circle on the curve, and coincide with the drawn PV curve if the Z_{Th} is estimated correctly.
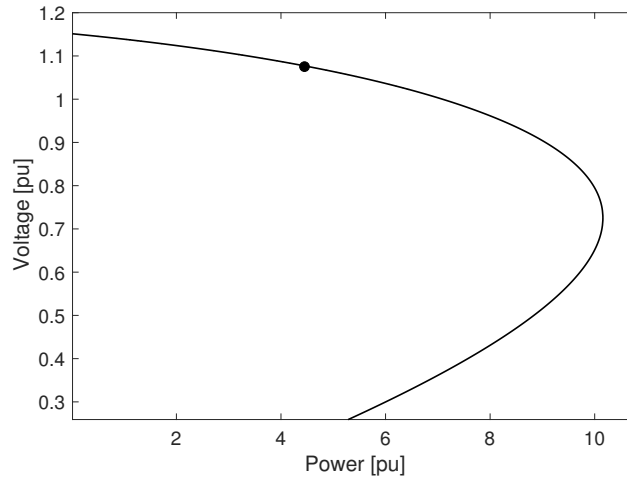
Figure 2.16: Corresponding PV curve drawn from the estimated Z_{Th} from Figure 2.15

2.7.5 Neglecting Complex Numbers in the Solution

The solution of the roots in equation (2.43) become a complex number during transients conditions. As it can be observed in (2.45), the last term of the root, becomes negative for low load current magnitudes. Low load current magnitudes can occur during large disturbance, for instance during short circuits or switching. The complex values have no physical meaning, and they are therefore neglected.

$$Z_{Th} = \frac{2\zeta cos\theta Z_L + \sqrt{(2\zeta cos\theta Z_L)^2 + 4(I^4 - \zeta^2)Z_L^2}}{2(I^2 - \zeta)} \tag{2.45}$$

2.7.6 Interpretation of the S-ZI

When the demand is increasing the load impedance is decreasing, $dZ_L < 0$. S-ZI describes the three different operating situations:

$$\text{S-ZI} = \frac{dS_L}{dZ_L} \begin{cases} < 0 & dS_L > 0 : \text{Power demand is met by the grid} \\ > 0 & dS_L > 0 : \text{Power demand is not met by the grid} \\ = 0 & dS_L = 0 : \text{Max. power demand the grid can supply} \end{cases}$$

At the operating condition where S-ZI < 0, the power is increasing, i.e. the grid manage to meet the power demand. At the second operating condition the power is decreasing, i.e. the grid can no longer meet the power demand. At the third operating condition, the power is not changing at all, meaning that the maximum loadability that the grid can supply is reached. The maximum loadability can be found as the critical P_{max} on the PV curve. S-ZI has a positive value at the upper part of the PV curve and a negative value on the lower part.

From equation (2.42) it can be observed that the term $(Z_{Th}^2 - Z_L^2)$ in the numerator, determines the sign of the S-ZI. It can be stated that for the different relationships between Z_L and Z_{Th}, the resulting S-ZI becomes:

$$\text{S-ZI} \begin{cases} < 0 & \text{when } Z_L > Z_{Th} \\ > 0 & \text{when } Z_L < Z_{Th} \\ = 0 & \text{when } Z_L = Z_{Th} \end{cases}$$

This coincide with the theory presented in Section 2.7.2 for the relationship between Z_L and Z_{Th}.

2.7.7 Filtering

Some of the data obtained will not be used for further analyses because of the occurrence of negative values, noise, etc. Therefore filtering the results is needed to analyse the data. This filtering includes the following:

- Only take into account situations where $dZ_L < 0$

- After S-Z sensitivity ζ is computed from dS_L and dZ_L, the signal must be filtered by applying a simple moving average filter

$$y[i] = \frac{1}{N} \sum_{j=0}^{N-1} x[i-j] \tag{2.46}$$

where x is the list of input samples, y is the resulting filtered output. N is the number of previous measurements that are used to calculate the unweighted mean.

32

3 | Combining Model and Measurement Based Methods for On-Line Voltage Stability Assessment

The work with this master thesis has in great part consisted of acquiring knowledge on the necessary software to perform these types of analyses. Therefore, an overview of the software and the utilisation of each of them is given. All source code will be made available in a ZIP file.

3.1 The Proposed Method

This master thesis will investigate how model and measurement based models can be combined to track the maximum loadability in a system, for on-line voltage stability assessment. The continuation power flow, presented in 2.6, and the S-ZI, presented in 2.7 are implemented for this purpose. Both methods estimate the maximum loadability at a *specific* load bus in the power system.
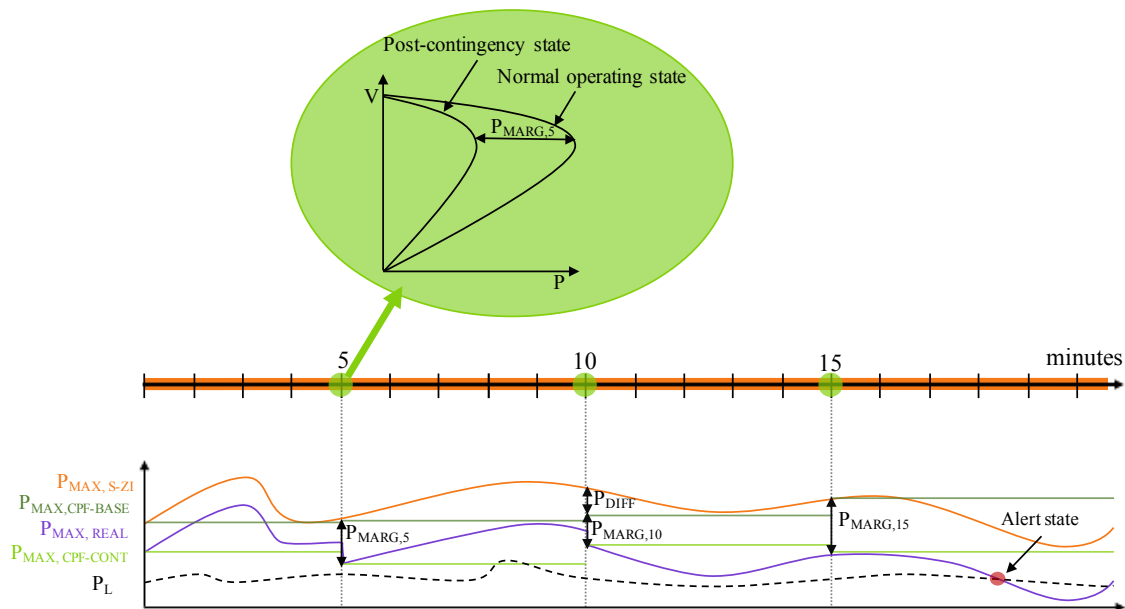
Figure 3.1: Proposed method

Figure 3.1 gives a graphical representation of the proposed method. The figure shows the load variation and the estimation of the maximum loadability limit, in a fictional power system, as they vary over a period of 20 minutes.

Five curves have been drawn in the graph. The black stippled line shows how the actual load, P_L, varies by time. The orange curve tracks the maximum loadability estimated by the calculated S-ZI, $P_{MAX,S-ZI}$. As the figure on top shows, $P_{MAX,S-ZI}$, is calculated continuously, i.e., as often as the PMU measurements are accumulated.

Every five minute, a continuation power flow is solved for the current system state. The CPF is solved for the normal operating state (i.e. the current operating state) and with a contingency added to the model. The maximum loadability after the contingency, $P_{MAX,CPF-CONT}$, is subtracted from the base case maximum loadability, $P_{MAX,CPF-BASE}$, to find the load margin, $P_{MARG,N}$, at the time step N.

$$P_{MARG,N} = P_{MAX,CPF-BASE} - P_{MAX,CPF-CONT} \tag{3.1}$$

The maximum loadability from CPF remains constant until the next time the CPF is solved for the new system state. The maximum loadability calculated by the S-ZI suggests that the maximum loadability might vary a lot, as the system is subjected to changes.

The maximum loadability estimated from the continuation power flow and the S-ZI, may not necessary coincide, as the time step 10 minutes exemplifies. The S-ZI estimates a higher P_{MAX} than the continuation power flow. This result in a difference in estimated maximum loadability of:

$$P_{DIFF} = P_{MAX,S-ZI} - P_{MAX,CPF-BASE} \tag{3.2}$$

All this combined creates the *"real"* maximum loadability limit for the system, $P_{MAX,REAL}$, where possible operating states with potential contingencies, are included. Equation (3.2) is set up under the assumption that the maximum loadability estimated by the CPF is more accurate than the one estimated from the S-ZI.

$$P_{MAX,REAL} = P_{MAX,S-ZI} - P_{DIFF} - P_{MARG,N} \tag{3.3}$$

As the figure shows, $P_{MAX,REAL}$ (given by the purple curve) gives an entirely different picture than the two methods do separately. At some time steps, the estimated maximum power limit from S-ZI indicates that the system has large power margins, while the CPF finds the system to be close to the limit. Between every time the CPF is solved, the system state can change a lot so that the maximum power limit estimated at the next time step, has changed so much that it can no longer be trusted. By combining the methods, the goal is to give the system operator an early warning of the system entering the insecure state.

When P_L crosses $P_{MAX,REAL}$, this is an indication to the system operator that the system is in an alert state (see figure). At this time, measures should be initiated to bring the system back to a secure state.

3.2   System Description

The system that will be considered in the case study in Chapter 4, is the Van Cutsem Nordic 32 [9]. The system was purposed by K. Walve and is a fictional system that bears a resemblance to the Swedish and Nordic system. All system data, operating points and contingency responses can be found in [9]. The on-line diagram of the system is presented in Figure 3.2, and the system operates according to system operating point A.

The system is divided into four areas, North, Central, South and Equiv. North is connected to Equiv and Central. Central is connected to South in addition to North. Equiv is the equivalent of an external system. The total generated and consumed (active) power of each area is presented in Table 3.1. Only the generators in North and Equiv are equipped with governors. North consist of hydro generation, and g20 in Equiv is an equivalent generator, which has high participation in the frequency control. Bus 10214, where g20 is situated, is also used as the slack bus in the load flow solutions.

Table 3.1: Active power generation and consumption [9]

Area	Power generation (MW)	Power consumption (MW)
North	4628.5	1180.0
Central	2850.0	6190.0
South	1590.0	1390.0
Equiv	2437.4	2300.0
Total	11505.9	11060.0

There are two properties, related to the distribution of the power generation and the power consumption in the system, that threaten the security of this system. North is the area with the highest amount of power generated. Central has a high load demand and is highly dependent on receiving power from the other areas, mainly from North.

Between Central and North, there can be found a clear transmission corridor, with the boundary buses 4031-4041, 4032-4044, 4032-4042 and 4021-4042. The tripping of any of the transmission lines between Central and North leads to higher strain on the remaining lines. The remaining lines may not even be able to transfer enough power to satisfy the load demand in the North, leading to voltage collapse in the system.

Central has five generating units, where g15 is the largest contributor (1200 MW), and g14 and g16 are the second largest (700 MW). The tripping of any of these generators will lead the speed governors in the North and Equiv to compensate, leading to additional power transfer (and strain) on the transmission corridor between North and Central.
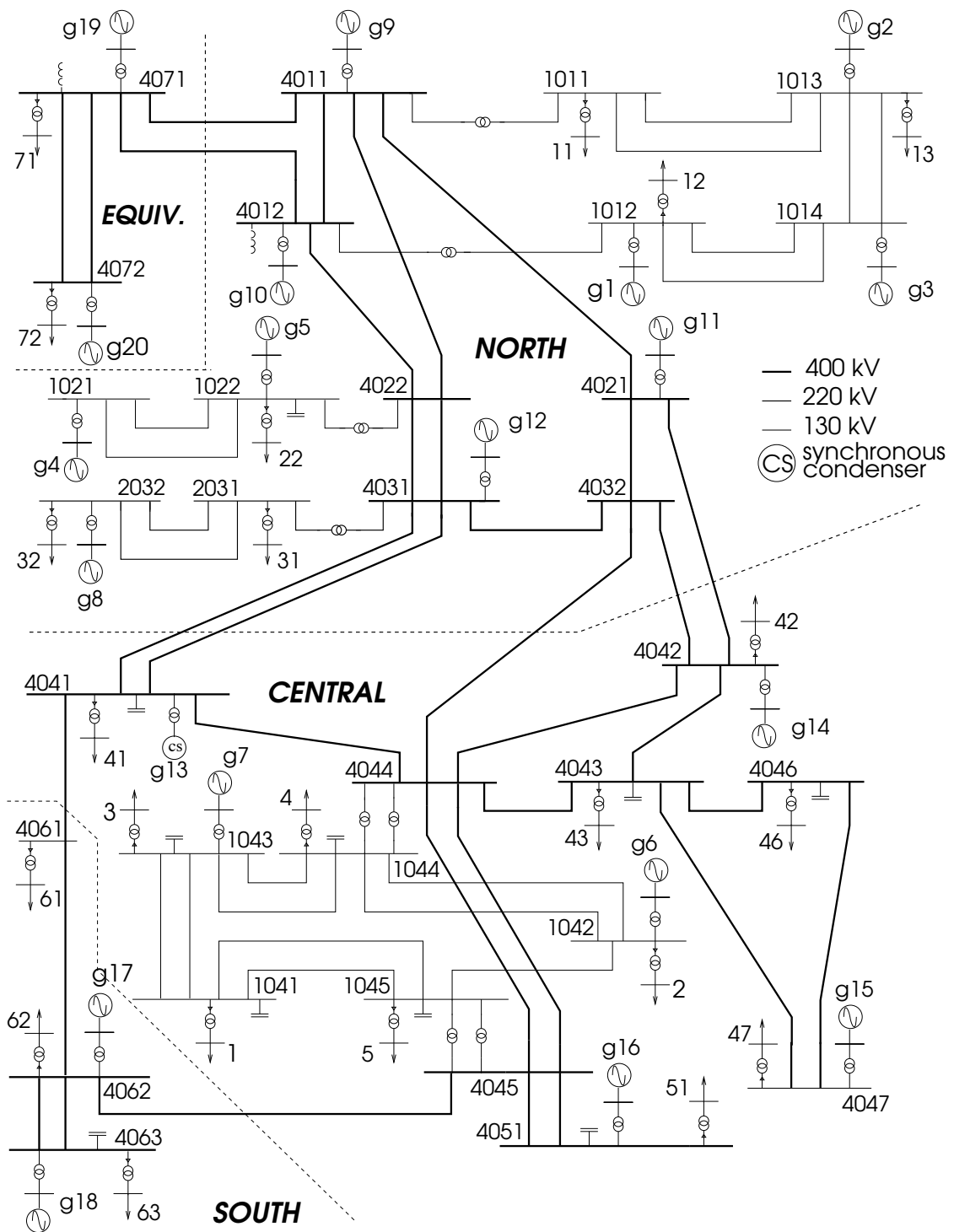
Figure 3.2: One-line diagram of Van Cutsem Nordic 32 [9]

3.3   Voltage Control of Bus 1

The proposed method from Section 3.1 will be tested on Bus 1 in Central. An initial study of the effect of available reactive power reserves in the system has been conducted. For this purpose, the FC at Bus 1041 is replaced by an SVC. The SVC to controls the voltage level at Bus 1 for different loading levels. In PSS/E, the SVC is added to the system as a generator, used to initialise the SVC in the power flow. The machine is equipped with the dynamic model for the SVC, CSVGN5. The block diagram of GSVGN5 is presented in Figure 3.3.
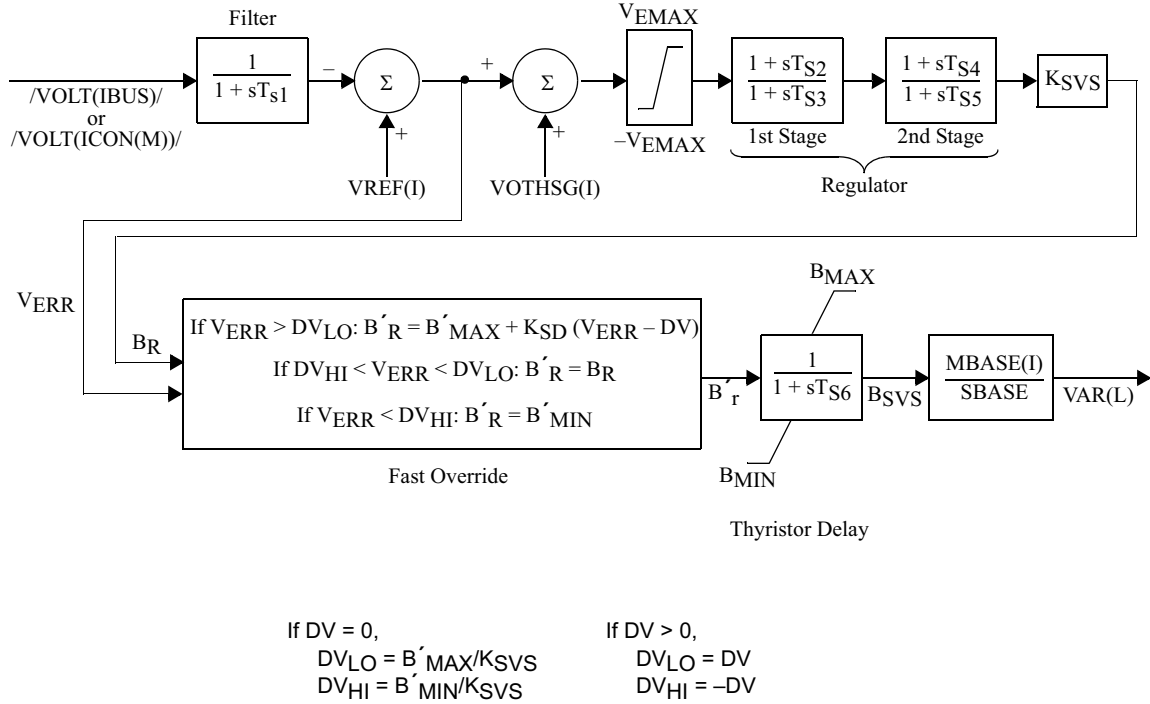
Figure 3.3: Block diagram CSVGN5

Table 3.2: Model Parameters CSVGN5 from Powerfactory

Parameter	Parameter Description	Value
V_{EMAX}	Error Signal Limiter [pu]	0.7
T_{S3}	Regulator 1st Stage Derivative Time Constant [s]	0.03
K_{KSV}	Regulator gain [pu]	200
B'_{MAX}	Fast Override Maximum Limiter [pu]	1
B'_{MIN}	Fast Override Minimum Limiter [pu]	-1
B_{MAX}	SVC Maximum Limiter [pu]	1
B_{MIN}	SVC Minimum Limiter [pu]	-1
T_{S6}	Thyristor Delay Time Constant [s]	0.03

The parameters of the CSVGN5 are first applied with the parameter values found in the system model library in Powerfactory (see Table 3.2). All other parameter values are set to 0 by default. With the applied parameter values, the control loop becomes a

Proportional-Integral (PI) controller. The block diagram takes in measurements of the bus voltage at Bus 1 and compares it to the desired voltage, VREF, which in this case is 1 pu. From this, it finds the deviation in voltage, VERR. The control loop takes in signals that are within the difference in measurements between -0.7-0.7 pu. The signal is amplified by the PI controller, to the resulting signal B_R.

The system is equipped with a fast override that maximises the reactive power support when VERR exceeds the maximum value given by DV_{LO} and when it exceeds the minimum value given by DV_{HI}. Since the *Fast Override Limiter*, DV, is set to 0 (by default), $DV_{LO} = B'_{MAX}/K_{SVC}$ and $DV_{HI} = B'_{MIN}/K_{SVC}$. Notice that *Fast Override Maximum Gain*, K_{SD} is zero, so that for the first condition, $B' = B'_{MAX}$.

To test the dynamic behaviour of the SVC two dynamic simulations were conducted, one to verify the model for a single step load increase, and one to test for a step-wise load increase. To optimise the control loop, the following changes were applied to the model parameters: B_{MAX}=1.3, B_{MIN}=-1.3, B'_{MAX}=1.2 and B'_{MIN}=-1.2.

3.3.1 Range of the SCV

Some load flows have been conducted at different loadings at Bus 1 (with constant power factor) to determine the operating range of the SVC. From a relatively high (initial) loading of 600 MW to a lower loading of 37.5 MW, the appropriate working range for the SVC is found to be in the range of -250 to 250 MVAr (see Table 3.3). If the load increases beyond 600 MW and 248.2 MVAr, the SVC can no longer offer sufficient voltage support to Bus 1.

Table 3.3: Reactive power demand from the SVC at different loading at Bus 1 (load flow results)

P_L Bus 1 [MW]	Q_L Bus 1 [MVAr]	Q_{SVC} Bus 1041 [MVAr]
600	248.2	247.4
300	74.1	-51
150	37.5	-168
75	18.25	-221.2
37.5	9.25	-248.8

3.3.2 Single Step Load Increase

The load demand at Bus 1 is reduced to 300 MW and 74.2 MVAr. The system is initiated by running a load flow, with the SVC supplying the system with 50.71 MVAr to set the bus voltage at Bus 1 equal to 1 pu at the loading of 300 MW and 74.2 MVAr. A load change of ΔP= 50 MW and ΔQ= 12.37 MVAr is applied to Bus 1 at time t=130 s.

The voltage response at Bus 1 to a sudden load increase of 50 MW, with and without an SVC at Bus 1041, is presented in the upper graph in Figure 3.4. Right after the load is increased, the voltage drops rapidly, before it stabilises at a higher value after some time. It can be observed that the SVC improves the voltage recovery a lot, compared to the case with only the FC. The SVC almost manage to bring the voltage back to 1 pu. The response of the SVC, regarding reactive power supplied/consumed, is presented in the lower graph. At the initial loading, the SVC *draws* reactive power from the system

(-50 MVAr). As the loading increases, more reactive power from the system needs to be allocated, and as a result, the SVC draws less reactive power. Initially, the reactive power consumed by the SVC is reduced to -7 MVAr, but after some time it stabilises at approximately -17.5 MVAr.
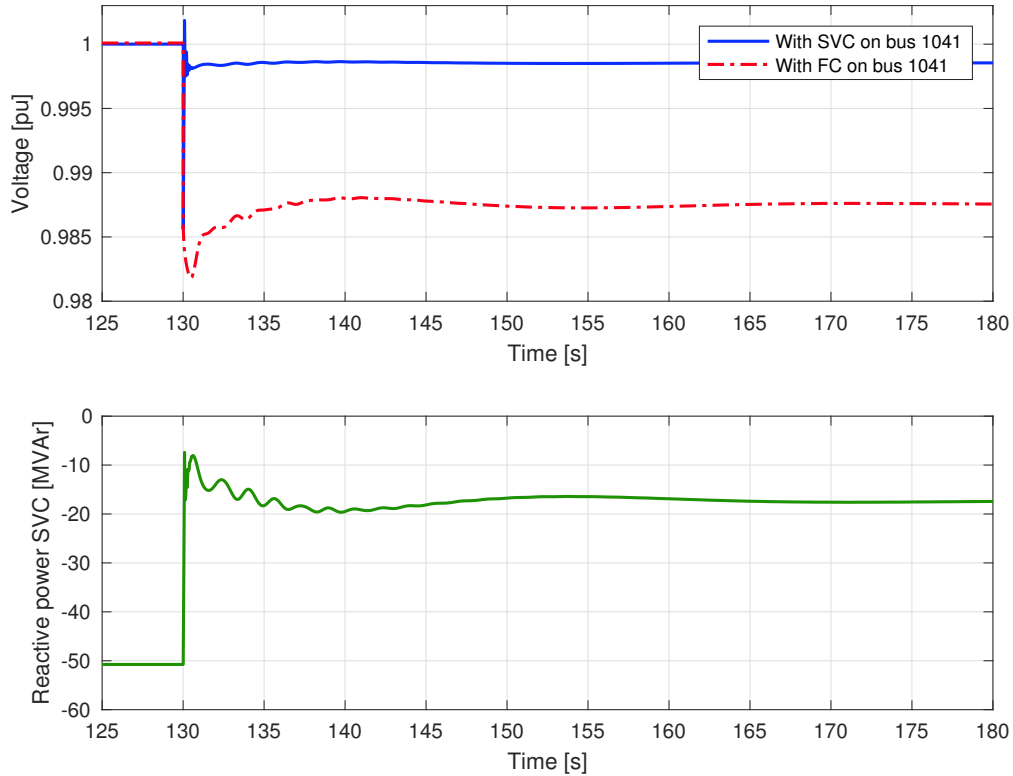
Figure 3.4: (Top) Voltage at Bus 1 after a sudden load increase with and without SVC (Bottom) Reactive power from the SVC at Bus 1041

3.3.3 Step-Wise Load Increase

The load is ramped up from 300 MW to 750 MW (and from 74.2 MVAr to 185 MVAr, keeping a constant power factor), during a time span of 15 minutes.

The voltage response at Bus 1 to a slow, step-wise increase of the load, with and without an SVC at Bus 1041, is presented in the upper graph in Figure 3.5. The voltage variation as a function of the loading at Bus 1 is plotted in Figure 3.6.

The green line shows the response when Bus 1041 have been equipped with an SVC. The SVC manages to supply the system with enough reactive power until time=452.5 seconds, at loading P_L=504.09 MW and Q_L=124.05 MVAr. Until this point, the voltage is kept very close to 1 pu. After this point, the voltage level decreases at a rapid pace.

The red dotted line presents the load scenario, without the SVC. The FC consumes 50 MVAr for the whole simulation period. The voltage drops at a constant rate and crosses the allowed voltage level ($\pm$ 10%) during the simulation period.

The reactive power supplied/consumed by the SVC on Bus 1041 is presented in the lower graph of Figure 3.5. As the graph shows, the SVC will only work for a given

operating range, according to its design and applied settings. Eventually, the SVC reaches
its maximum capacity limit and is unable to supply more reactive power to the system.
As a result, the voltage at Bus 1 starts to decrease.
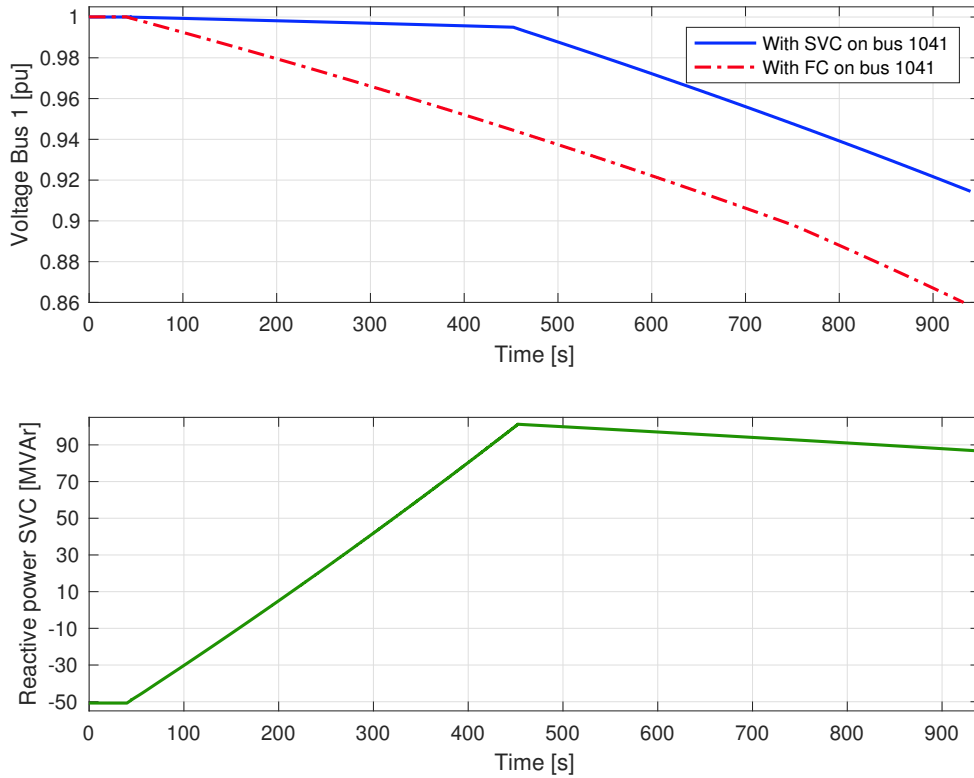
Figure 3.5: (Top) Load increase at bus 1, with SVC and with FC (Bottom) Reactive power
from the SVC
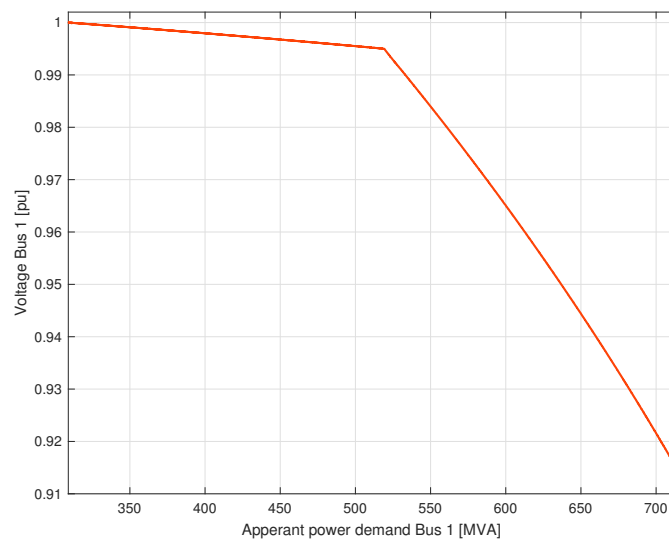
Figure 3.6: PV curve Bus 1.

Figure 3.7 shows the PV curves for some time steps estimated from the calculated Z_{Th} from the same simulation. As long as the SVC supplies more reactive power the next operating point moves vertically along the x-axis, and the estimated P_{MAX} increases. All other variables in the system remain unchanged during the simulation period. The grey stippled line indicates the working area of the SVC, and thus the path that the voltage will follow while still receiving voltage support. When the SVC cannot supply more reactive power (and becomes a fixed reactor), the next operating point plotted follows the curvature defined by the previous operating point. The estimated P_{MAX} becomes smaller for the two next time steps (t=501 s., t=563 s.). The last time step has a larger P_{MAX} than the previous one.
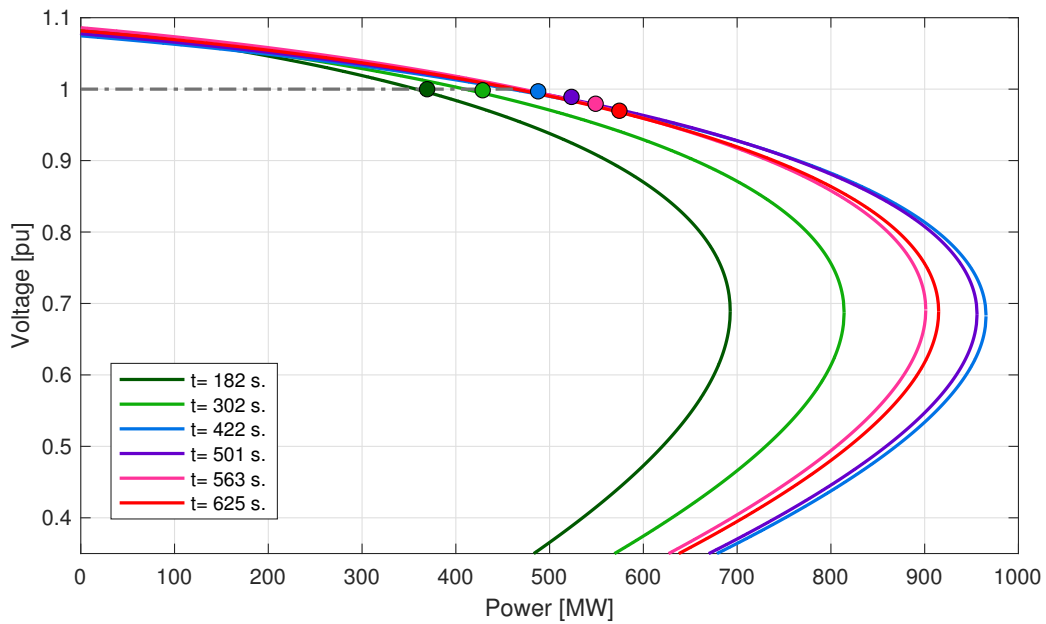
Figure 3.7: Resulting PV curves at some time steps

3.4 Implementation of the Dynamic Simulation and the Methods

3.4.1 Software

The following software, with the given versions of them, has been used to perform the case study that will be presented in Chapter 4. An overview of how the software have been applied (and in what order) is given in the flow chart in Figure 3.8. A more detailed description of how the different parts have been implemented will be provided in the next few sections.

PSS/E version 33.6.0
PSS/E is a power transmission system planning software by Siemens. Both dynamic simulations and load flows have been conducted using PSS/E with the Van Cutsem Nordic 32 power system, presented in Section 3.2. The dynamic simulations were done running PSS/E from Python.

Python version 2.7.6
Python is an object-oriented, high-level programming language, with a simple syntax that aims for the code to be easily read. The dynamic simulations have been conducted in Python, by importing PSS/E appliances and output to Python. A presentation of the commands that have been applied in Python will be given in Appendix A.1.

MATLAB®R2016b
MATLAB is a matrix-based programming language with a lot of built-in graphics. The S-Z sensitivity indicator has been implemented in MATLAB, as well as all the graphical representations that will be presented in the Chapter 4.

MATPOWER version 6.0
MATPOWER is a MATLAB®Power System Simulation Package that consists of m-files that can solve power flows and optimal power flows. It is developed for research and education, and it is simple to use and edit, but does lack some of the possibilities that you find in real programs like PSS/E and Powerfactory. For this work, it has been used to run continuation power flows.

3.4.2 Dynamic Simulation in PSS/E

This section will present how the case study in Chapter 4, was done, regarding the coding done in Python. The structure of the simulation that was performed is given in Figure 3.8

The PSS/E user manuals for Application Program Interface (API) [10] have been used to find the necessary commands from Python to PSS/E, also [28] have been used to find the correct syntax for Python. A detailed overview of all the functions that have been used, and the applied settings, is given in Appendix A.1.
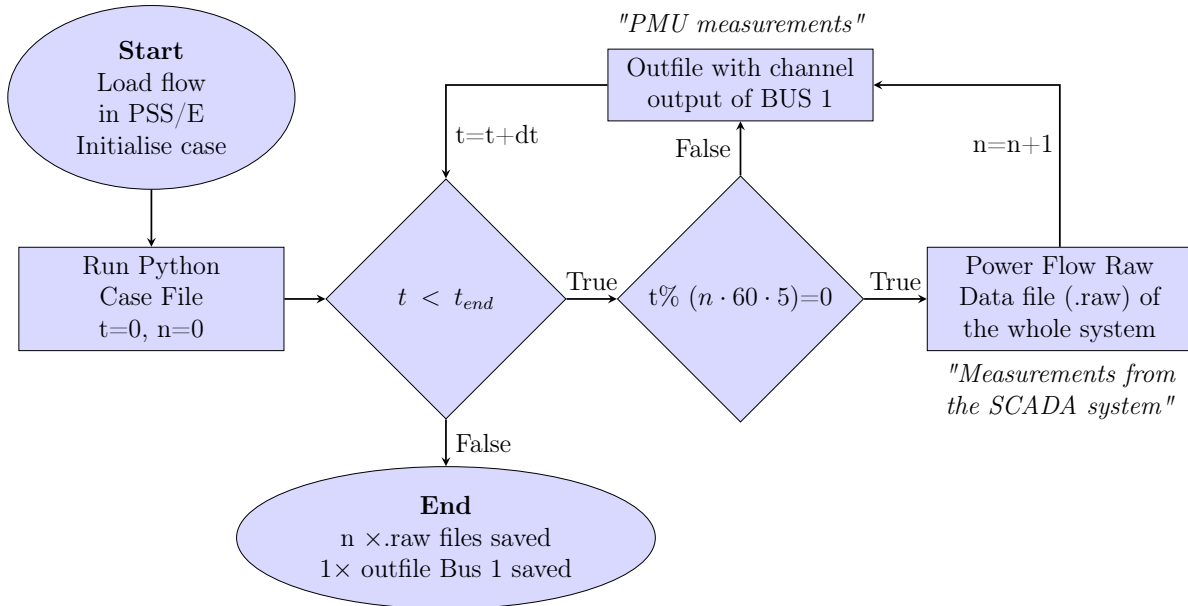
Figure 3.8: Simulations in Python

The S-ZI only works when the load demand is increasing at the load bus that is studied. The load at Bus 1 is reduced from 600 MW and 148.4 MVAr to 550 MW and 135.85 MVAr, and a small increase in load back to the initial loading. To properly initialize the PSS/E Saved Case (.sav) at the new loading, a load flow is run. The generators are converted to ZSOURCE, and the loads are converted to constant MVA loads with the active power as constant current load and reactive power as constant admittance load. The .sav file and its subsidiary Dynamics Model Raw Data (.dyr) File are read into the PSS/E working case. At the beginning of the simulation, the end time of the simulation, t_{end}, is given. While the time t is less than t_{end}, bus quantities for Bus 1 are saved in an output file. These are the *PMU measurements* of the bus in the case study. Measurements are collected every 40 ms, which is the standard rate of data accumulated from a PMU.

To uniformly increase (or decrease) a bus quantity of a specified bus or group of buses (defined as *SID*), can be performed by the API *SCAL*.

The scaling target can be set to the total new specified total power, percent change or incremental change power demand. The S-ZI presupposes a constant power factor at the studied load. For simplicity, constant power factor is set for the change in load demand at the other buses as well. To slowly ramp up the load demand, the *SCAL* is applied using a for-loop, with a time step of 1.2 seconds. The time step must be long enough to allow the system to adjust to the small change in load, but small enough to get an approximately

uniform increase. To get the desired time step, dt, the resulting number of steps can be
found by dividing the total simulation time (in seconds) by dt (also in seconds).

For a total increase of 10 % of initial power load, the load needs to be increased by
$(x - 1)$ every step:

$$P_{L,final} = 1.1 \cdot P_{L,initial} = x^{steps} P_{L,initial} \tag{3.4}$$

Solving (3.4) with respect to x:

$$x = 10^{\frac{log(1.1)}{steps}} \tag{3.5}$$

The *SCAL*-function takes in increase in load demand in percentage of the current load
demand. The input value therefore becomes:

$$\Delta P_\% = (x - 1) \times 100\% \tag{3.6}$$

A Power Flow Raw Data (.raw) File of the system is saved every five minutes. The
.raw file contains measurements of the whole system, and will be regarded as the *SCADA
system measurements* of the system in these studies. Since a for loop is used to apply
the load increase, it is possible to keep track of the time t, using an if-statement with a
modulo operation. Given to positive numbers, a divided by n, the modulo operation gives
the reminder of a Euclidean division. For instance, if a equal 5 and n 2, the remainder
becomes 1. In Python, the modulo operation is given by %, and the condition in the if
statement to only save a .raw file when t%(60 · 5)==0, i.e. only when five minutes (or
$(5 \cdot 60$ seconds) have passed).

3.4.3 Continuation Power Flow

The continuation power flow is performed using the inbuilt function in the MATPOWER
library. First, the .raw file from the dynamic simulations is imported and converted to a
MATPOWER case struct (mpc) file. An output .raw file is a replication of the current
working case, which in this case is "*snapshot*" of a dynamic simulation. In the dynamic
simulations in PSS/E, no bus is defined as the slack bus. In the original .sav file in PSS/E,
Bus 407220 is set as the slack bus before the generators and loads are converted. Bus
407220 is situated in Equiv, and generator g20 is connected to the bus. Generator g20
is, as mentioned in 3.2, an equivalent generator of Equiv with large capacity. The bus is
situated from a reasonable distance to the Bus 1, and will, in this case, be an appropriate
choice as the slack bus for the load flows in the continuation power flow.

The SVC, placed on Bus 1041, will be considered as an ordinary generator by MAT-
POWER, controlling the voltage at Bus 1, which will prevent the continuation power flow
to work accurately. Bus 1041 is first converted from a PV bus to a PQ bus. The generator
is replaced by a shunt susceptance, injecting the same amount of reactive power to the
bus.

The following settings have been applied to the MATPOWER continuation power flow solution:

- Parametrisation: Pseudo arc length

- Step size: 10^{-4}

- Adaptive step size enabled

- Maximum allowed step size: 0.2

- Constant power factor

Figure 3.9 show an example of the steps with the applied method. Around the tip of the curve, the adaptive step size enabled, allows the CPF to use smaller steps here, to create a more accurate curve, and find a better approximation for maximum loadability (nose point).
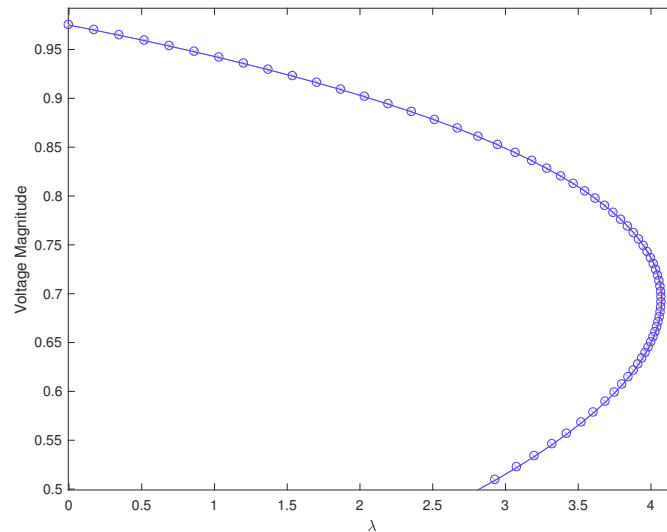
Figure 3.9: Example of CPF with the applied settings

It should also be noted that the load is no longer constant current and constant admittance load when they have been converted to a mpc. When the file is converted, the loading becomes different. The load is changed manually to a constant power load in the .raw file to ensure that the loading at Bus 1 is the same as in the dynamic simulation. A detailed overview of functions that have been used from MATPOWER and the structure of a MATPOWER case struct is given in Appendix A.2 or see [29].

3.4.4 S-ZI

The S-ZI has been implemented in MATLAB in accordance to the theory presented in Section 2.7. The resulting outfile from the dynamic simulations in PSS/E are used as the PMU input measurements at Bus 1.

To verify the predetermined X_{Th}/R_{Th} the trajectory must be drawn for the resulting Z_{Th}. By testing for different values of the X_{Th}/R_{Th} ratio, 4.1 was found to be a good approximation. Figure 3.10 shows some resulting trajectories drawn at different time steps in the case study.
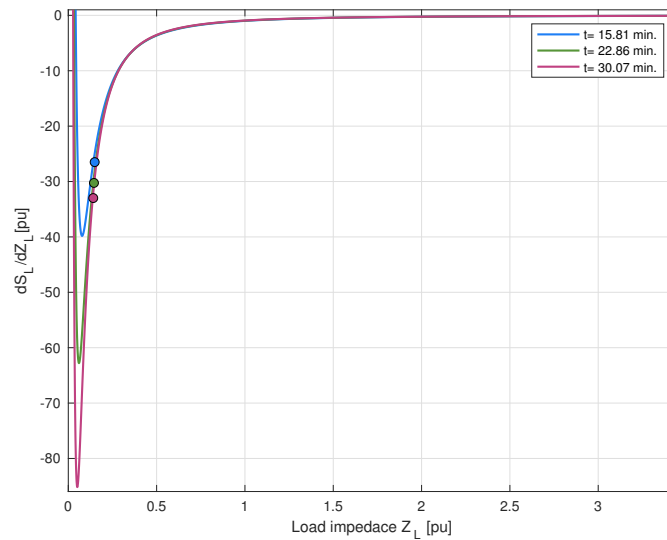
Figure 3.10: Drawn trajectories at some time steps in the case study

When the X_{Th}/R_{Th} has been verified, the resulting PV curve for the current operating state can be drawn. PV curves at the same time steps have been plotted in Figure 3.11.
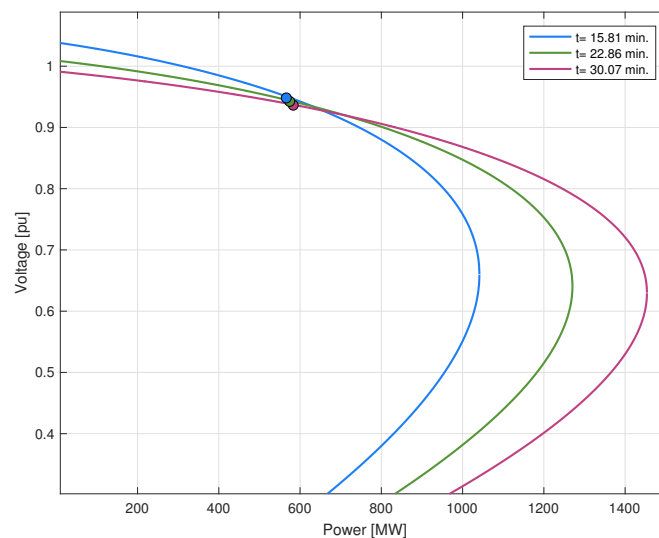
Figure 3.11: Resulting PV curves from the estimated Z_{Th} at some time steps in the case study

4 | Case Study: System Approaching Voltage Collapse

The proposed method in Section 3.1 will be tested by studying the impact of two consecutive contingencies in in the system (Van Cutsem Nordic 32), seen from Bus 1 in Central. In the specialisation project [12], the system stability after the tripping of the line between Bus 4032 and Bus 4044 was investigated. Through dynamics simulations, the system was found to be unstable at the loading of Bus 1 of 600 MW and 148.2 MVAr. The case study is set up with the intention of assessing the stability of the system at different stages, with the two methods and with the proposed method, as the system approaches system collapse.

4.1 Case Description

Before the case study was conducted, the following changes were applied to the Van Cutsem Nordic 32 system in PSS/E:

- Initial loading at Bus 1 is set to be 550 MW and 135.85 MVAr, all other quantities remain unchanged (referred to operating point A).

- The capacitor bank on Bus 1041 is replaced by an SVC, for improved voltage control of Bus 1.

- A new generator, g18b, is placed on Bus 4063 in South. g18b is applied with the same properties as g18, which is also situated on the same bus. The transformer connecting g18b to Bus 4063 is implemented likewise.

- Load restoration is added to the system by adding an Extended-Term Load Reset Model to all the loads in the system (see Appendix A.3).

The collection of data in the system is done in two ways:

- Measurements of the bus quantities at Bus 1 (bus voltage, active and reactive load demand) is accumulated every 40 ms.

- Measurements of the whole system is collected every five minutes.

The following case study is to be conducted in PSS/E:

1. 10% increase of the active and reactive power at Bus 1 is applied step-wise, from the simulation start

2. Generator g18b is tripped after 31 minutes and remains tripped throughout the rest of the simulation period.

3. The line between Bus 4032 and Bus 4044 is tripped after 46 minutes due to a short circuit on the line. For simplicity, the short circuit is not included in the simulation.

4.2 Results

Figure 4.1 show the resulting voltage at Bus 1 throughout the simulation time. The voltage drops from simulation start, indicating that there are not enough reactive reserves in the system. The tripping of the generator at 31 minutes, is only seen as a small oscillation but stabilises after not too long. When the line is tripped, the voltage falls and oscillates before it collapses.
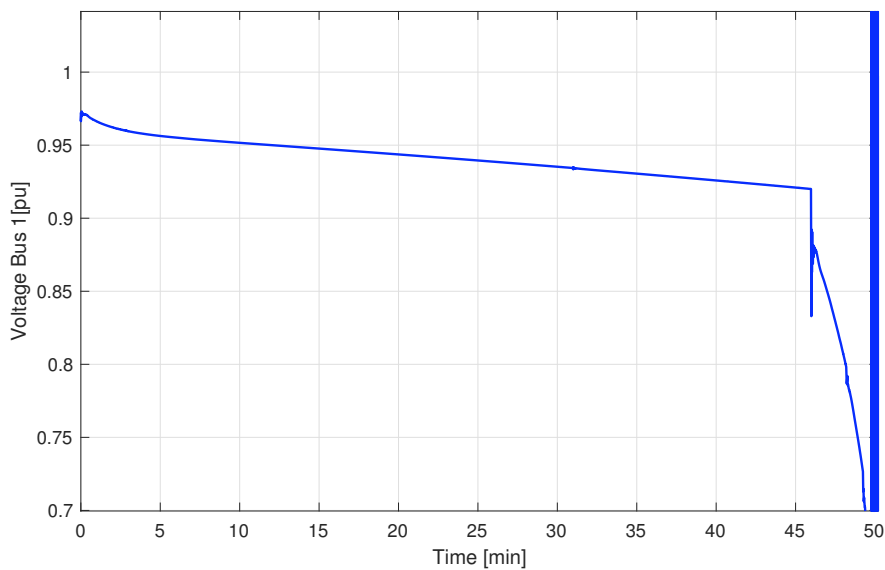
Figure 4.1: Voltage at Bus 1

Figure 4.2 show the increase in active power demand. The power demand increases uniformly until about 605 MW when the line is tripped. After the line is tripped, the system can no longer supply the demanded power, and the system struggles to bring the loading back, but eventually collapses.
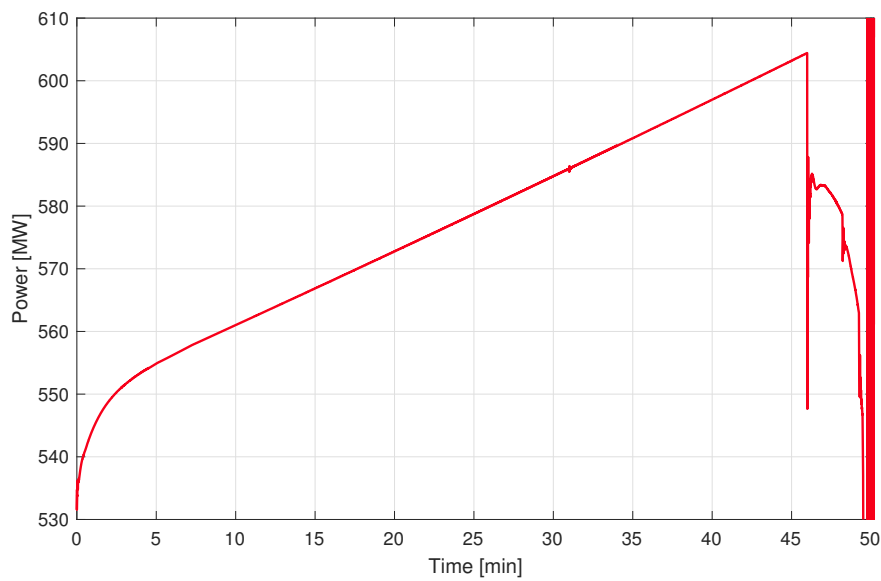
Figure 4.2: Power demand at Bus 1

Figure 4.3 shows how the voltage varies as the load increases in the simulations, forming the *real* PV curve of Bus 1. The voltage can be seen to change linarly with the increase of power until the system collapses.
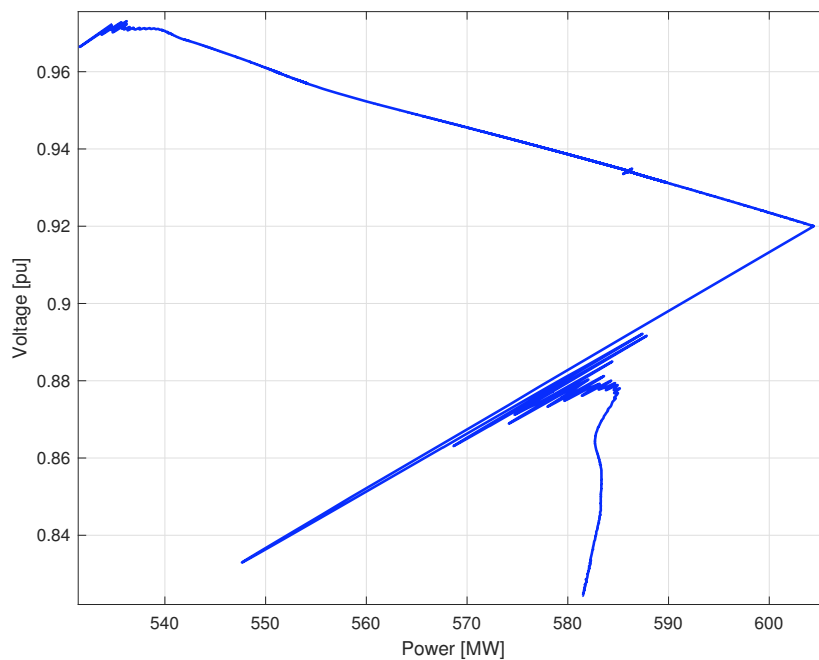
Figure 4.3: *Real* PV curve of Bus 1 based on the simulation results

The estimated S-ZI is drawn in Figure 4.4, the indicator crosses the stability limit (zero) after about 46.5 minutes, indicating that the system can no longer sustain the load. The tripping of a generator g18b can be found as the distinctive "spike", and the value of the indicator settles at a higher value than before after the generator has been tripped.
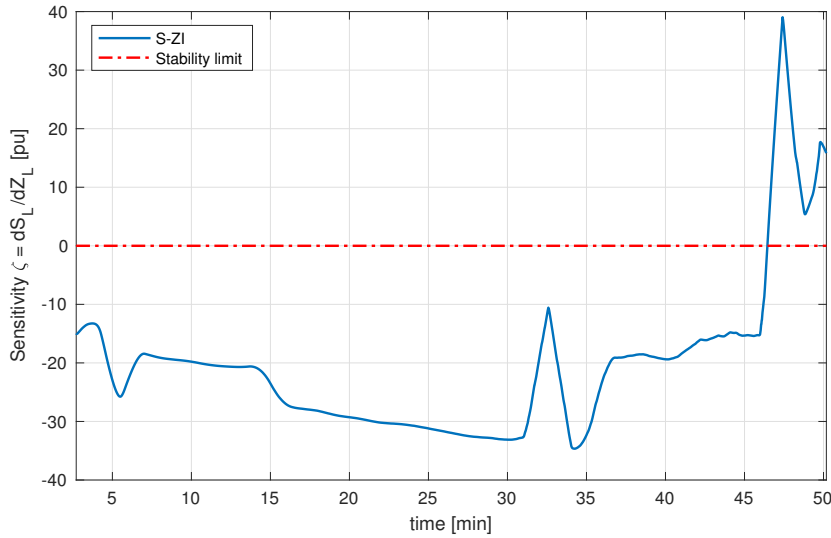
Figure 4.4: S-ZI estimated from PMU measurements at Bus 1

In Figure 4.5 the real Z_L and the calculated Z_{Th} is drawn as they vary by time. Z_L decreases as the loading increases. The value of Z_{Th} needs time to settle and first become relatively constant after approximately 16-17 minutes. The Z_{Th} can bee seen to follow the shape of the SZ-I. When generator g18b is tripped after 31 minutes, Z_{Th} have a rapid increase, followed by a decrease back to the previous value, before it settles at a higher value. When the line is tripped Z_{Th} crosses Z_L, and Z_L becomes smaller than Z_{Th}.
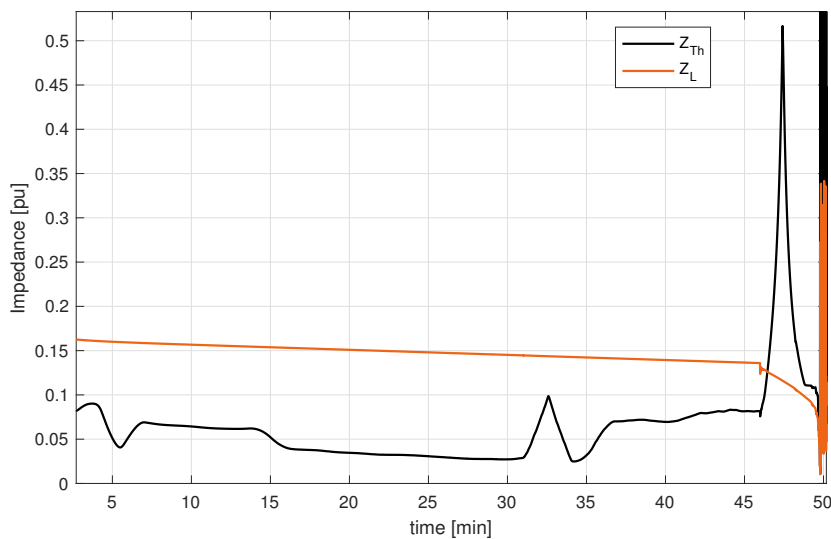
Figure 4.5: Z_{Th} and Z_L

Figure 4.6-4.8 present PV curves, based on the S-ZI (and the resulting Z_{Th}), and PV curves estimated by CPF. The *current* operating point is indicated by the red dot and the PV curve estimated by S-ZI is indicated by the black curve. The CPF is executed for two operating states, one with the current operating condition (blue curve) and one without the line between Bus 4032 and 4044 (green curve).

The CPF converged for both the base case and the contingency at the time steps: 10, 30, 35 and 40 minutes. At time 15 minutes, only the base case converges, and at time step 5 and 20 minutes, only the CPF after the line is lost converges. The estimated P_{MAX} at the different time steps is presented in Table 4.1. Since the Z_{Th} first settles at a constant value after 16.5 minutes, the CPFs for the 3 first time steps will not be considered for comparison.

Table 4.1: Estimated maximum loadability from SZ-I and CPF

Time [min]	$P_{MAX,S-ZI}$ [MW]	$P_{MAX,CPF,pre-cont.}$ [MW]	$P_{MAX,CPF,post-cont.}$ [MW]
5	903.91		612.66
10	773.15	808.22	693.96
15	885.21	814.80	
20	1204.79		671.15
25	1321.74		
30	1455.76	827.48	721.21
35	1268.84	836.31	733.07
40	738.21	840.87	740.12
45	687.62		

Figure 4.6 shows the situation of the system after exactly 30 minutes. $P_{MAX,SZ-I}$ estimated by the calculated Z_{Th} is a lot higher than for P_{MAX} estimated by the CPF. According to the CPF after the loss of line of 4032-4044, the system is close to the maximum loadability, and the stability limit. The CPF solves the case so that the voltage at the bus is 1 pu at the starting point for the base case scenario.
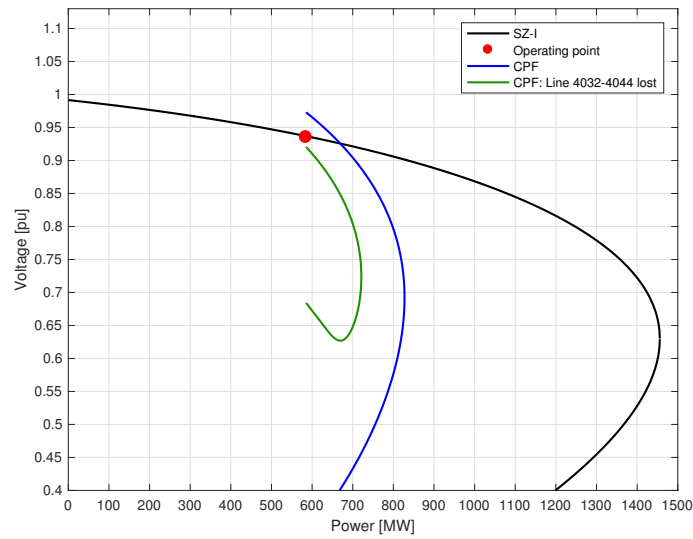
Figure 4.6: PV curve from case study, at time step t=30 minutes
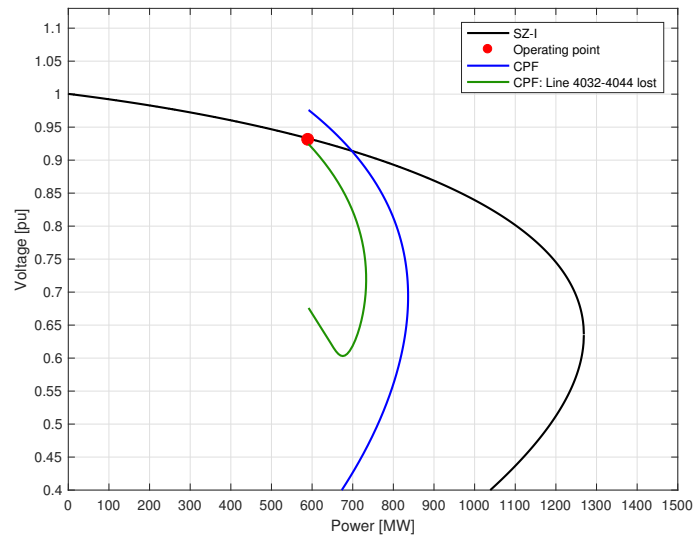
Figure 4.7: PV curve from case study, at time step, at time step t=35 minutes

At time step t=35 minutes the $P_{SZ-I,MAX}$ have become smaller compared to the previous time step. $P_{MAX,CPF-BASE}$ and $P_{MAX,CPF-CONT}$ have increased a little bit (see Table 4.1, even though it is not very noticeable in the figure).
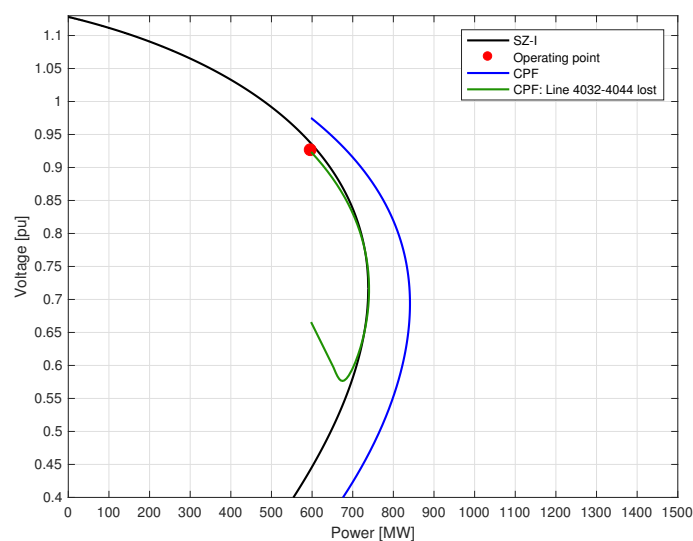
Figure 4.8: PV curve from case study, at time step t=40 minutes

Figure 4.8 shows the last time step, t=40 minutes, at which CPF has been solved. $P_{MAX,CPF-BASE}$ has become bigger than $P_{MAX,S-ZI}$, and $P_{MAX,S-ZI}$ and $P_{MAX,CPF-CONT}$ have become approximately the same. The PV curve from the CPF, post-contingency, almost coincides with the curve drawn on the basis of $P_{MAX,S-ZI}$.
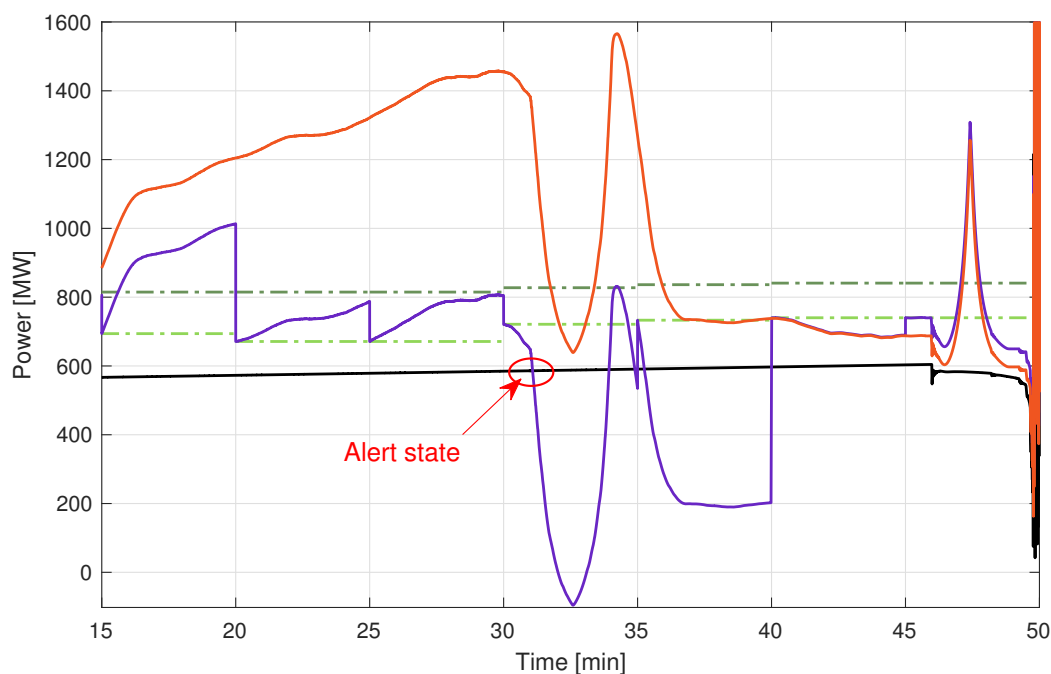
Figure 4.9: Case study results for maximum loadability $P_{MAX,REAL}$ (purple), $P_{MAX,S-ZI}$ (orange), $P_{MAX,CPF-BASE}$ (dark green) and $P_{MAX,CPF-CONT}$ (green) and load P_L (black)

Figure 4.9 show the estimated $P_{MAX,REAL}$(purple curve), that have been estimated according to the proposed methods presented in Section 3.1, together with the estimated maximum loadability from the two methods and the real loading (black curve).

The estimated maximum loadability estimated from the S-ZI, $P_{MAX,S-ZI}$, is not a constant variable and changes at every single time step. After the Z_{Th} settles (time>15 minutes), the estimated maximum loadability increases (up to a maximum value of more than 1400 MW) until generator g18b is tripped. The loadability increases rapidly for 2.5 minutes after the generator is tripped before it drops down to a much lower value.

The estimated maximum loadability from CPF, with the base case and after the line is tripped plotted with dark green and green. They remain constant until they are estimated the next time step. For the CPFs that could not be solved, the previously estimated value is used. The resulting values for $P_{MAX,SZ-I}$, P_{DIFF}, P_{MARG} and $P_{MAX,REAL}$ at every step the CPF is solved (or attempted solved) is presented in Table 4.2. The estimated $P_{MAX,REAL}$ does not remain at the estimated value but will vary with the change of $P_{MAX,SZ-I}$. Every time a new value of $P_{MAX,REAL}$, it is like a *re-calibration* of the estimated $P_{MAX,REAL}$ to the new system state.

With the proposed method the system is found to move into the *alert state* (stable and insecure) after the generator is tripped when P_L can be seen to cross the estimated $P_{MAX,REAL}$.

Table 4.2: Calculated values of $P_{MAX,SZ-I}$, P_{DIFF}, P_{MARG} and $P_{MAX,REAL}$ at every time step the CPF is conducted

Time [min]	$P_{MAX,SZ-I}$ [MW]	P_{DIFF} [MW]	P_{MARG} [MW]	$P_{MAX,REAL}$ [MW]
10	773.15	-35.08	114.27	693.96
15	885.21	70.41	120.84	693.96
20	1204.79	389.99	143.65	671.15
25	1321.74	506.94	143.65	671.15
30	1455.76	628.27	106.27	721.21
35	1268.84	432.53	103.24	733.07
40	738.21	-102.66	100.75	740.12
45	687.62	-153.25	100.75	740.12

5 | Discussion

In the case study generator g18b is added to the South-Central area, to make it more self-sufficient, and less vulnerable to the tripping of any of the transmission lines to the North-Equiv area. The simulation runs for some time before the generator is tripped since it takes time for the estimated Z_{Th} to stabilise at a relatively constant value, see Figure 4.5. In real power systems, Z_{Th} cannot be assumed to take on a constant value, but given that all other system variables (except loading at Bus 1 and the reactive output from the SVC) remain relatively constant, it is a reasonable to assume it for the case study. After 15-16 minutes the Z_{Th} settles at a value that remains constant until generator g18b is tripped (after 31 minutes).

Around the same time as Z_{Th} settles at a constant value, the estimated $P_{MAX,SZ-I}$ can be seen to increase as the simulation proceeds (see orange curve in Figure 4.9). From an estimated $P_{MAX,SZ-I}$ of 885 MW after 15 minutes, it increases up to 1455 MW right before g18b is tripped. The CPF, for the solvable time steps, finds a much lower estimated maximum loadability (see Table 4.1), but it is also increasing for the subsequent CPFs. In CPF, its solution scheme does not "know" about the reactive power that is still available in the system, and the solution will change as more or less reactive power is supplied to Bus 1041. At the last converged CPF before generator g18b is tripped (30 minutes), the estimated $P_{MAX,SZ-I}$ is 1.7 times as big as $P_{MAX,CPF-BASE}$ and more than twice as big as $P_{MAX,CPF-CONT}$.

When the generator is tripped it is detected by the S-ZI as a distinctive "spike" at the time it occurs (see Figure 4.4). Afterwards, the Z_{Th} settles at a higher value, resulting in a much lower estimated $P_{MAX,S-ZI}$. The loss of the available generation has no or little impact on the solution of the CPF (see Figure 4.6 and 4.7), and the estimated $P_{MAX,CPF-BASE}$ and $P_{MAX,CPF-CONT}$ continue to increase. The next CPF conducted happens four minutes after the generator is tripped, and it is possible that the system has managed to settle during that time. Nevertheless, it is impossible to detect that something has happened to the system by only looking at the resulting PV curves from the CPF.

After 40 minutes, the estimated $P_{MAX,SZ-I}$ from the S-ZI has become smaller than $P_{MAX,CPF-BASE}$, and it is almost the same as $P_{MAX,CPF-CONT}$ (see Figure 4.8) . The curve created by the estimated $P_{MAX,S-ZI}$, coincides with the curve set up by the CPF, for post-contingency state, around the tip of the PV curve.

The CPF could not converge at the time step 45 minutes, which is the last time step it can be solved before the line is tripped. There are two possible reasons for the CPF not to be solvable: 1. The system is too close to the maximum loading limit so that the CPF cannot converge for any further increase in the load. 2. At some of the time steps the CPF solution does not converge, as previous time steps show (see Table 4.1).

Most likely it is due to the first reason, and this identifies one of the challenges when only relying on CPF. The CPF is only applicable as long as the system is at a certain distance from the stability limit. When the system is too close to the stability limit, the CPF cannot find a solution for maximum loadability. At some of the earlier time steps, CPF could not be solved. Even if the system is stable, one single "snapshot" of the system may not be when solving the CPF. When the CPF cannot be solved, this leads to a time gap where the system operator does not know the current operating state of the system.

The accuracy of the S-ZI becomes better for higher loading, and the closer the system is to the stability limit. The only time of which the calculated $P_{MAX,S-ZI}$ from the S-ZI can be considered as certain, is when $Z_L=Z_{Th}$, i.e. when the load is equal to the maximum loadability. From the real PV curve (Figure 4.3), the system is found to collapse as the line is tripped. In Figure 4.8, the estimated $P_{MAX,SZ-I}$ is almost equal to P_L at the time of tripping the line, supporting this. At that time, the loading is 604.42 MW. For the previous time steps, both methods have overestimated the maximum loading limit. The first solution that was solved after 5 minutes, for CPF, post-contingency, is the closest value.

In the resulting CPFs, once the voltage at Bus 1 begins to deviate from 1 pu, the starting point of the CPF begins to deviate. The load flow will try to be solved such that all bus quantities equal to 1 pu creating a different path.

The proposed method, combining CPF and S-ZI is presented in Figure 4.9. When g18b is tripped the proposed method detects that the system has moved into the alert state when the estimated $P_{MAX,REAL}$ crosses the loading, P_L. It tells the system operator that the system is not stable if the line between Bus 4032 and 4044 is tripped, and gives him/her an opportunity to set in countermeasures.

The proposed method is, to a certain extent, able to combine the strengths and weaknesses to the two methods. The CPF can estimate a more accurate maximum loadability, but is less reliable, since it depends on measurements from the whole system. SZ-I cannot be used to estimate a good maximum loadability but can detect changes in the system. The proposed method is best applied long term. When it detects a problem, it should be dealt with at once. After it has detected the problem, it is found to be stable again after some time, even though the operating state remains unchanged.

Both the methods are based on simplifications. The S-ZI (and the resulting Z_{Th} and $P_{MAX,S-ZI}$) is based on a simplified two bus system, where the whole system connected to the load bus, is viewed as a Thevenin voltage source and Thevenin impedance. At the beginning of the simulation, an X/R ratio is set to a constant value, but the system topology will change, as well as the available generation, and the load demand. The X/R ratio will change due to the changes in the system, and in practice, it is not possible to estimate an accurate value of Z_{Th}. In CPF, the system is simplified to a steady state model, discarding system dynamics. In real EMSs, CPF is based on systems that are often simplified. The input measurements to CPF are filtered by SE, to find measurements that are suitable for assessment. The uncertainty in measurements have not been considered in these simulations but will contribute in forming two very different *"systems"* for assessment. At the same time steps, CPF and S-ZI do not find the same maximum loadability, and when including the contingency in the CPF, assumptions must be made to whether $P_{MAX,SZ-I}$ or $P_{MAX,CPF-BASE}$ is the most accurate estimated value. As long as the system is far enough away from the stability limit CPF is more accurate, but close to voltage collapse $P_{MAX,SZ-I}$ will become more and more accurate.

In real power systems, voltage controls are applied continuously, to keep the bus voltages within given limits. To simulate reactive power reserves in the system, an SVC was added to the bus outside of Bus 1. Reactive power reserves in the system make it possible to change the loading, keeping the voltage level constant. The SVC added to the system was set in the operating range of -250 to 250 MVAr and manages to maintain the voltage constant up to a loading of 525 MW (see Figure 3.6). As shown in Figure 3.7, the voltage control increases the estimated P_{MAX} calculated by the Z_{Th}.

Because of economic considerations, reactive power reserves cannot work for all possible operational points, and the operating range must be chosen to work within the most common range in loading. When the reactive power demand in the system surpasses the SVC's maximum capacity limit, the SVC can be considered as an fixed reactor (FR), as it will continue to supply at maximum. In the case study, a loading that is higher than the operating range have been applied, so that there are no more reactive power reserves available.

6 | Conclusion

This master thesis has considered the possibility of combining measurement and model based methods for on-line voltage stability assessment in the power system. A proposed method combining the S-ZI and the CPF have been presented and implemented in a case study.

The CPF needs measurements from the whole network, in addition to system models of all system components. Since the CPF uses a system model, it is possible to make changes in it, to predict possible future states. The CPF requires a lot of input variables, as well as many computational steps to find a solution, which makes it both time consuming and very computational demanding. It is, therefore, not desirable, or even possible, to perform the CPF very often. It leaves long time gaps between each computation, and events that occur in the system may go unnoticed by the CPF. The S-ZI is calculated directly using consecutive measurements on the bus connected to the load, assessing the stability of the current operating state and detecting it if the system approaches the stability limit.

The idea behind the proposed method was to combine the accuracy of the CPF, with the frequency of S-ZI. The resulting maximum loadability varies as the S-ZI changes but is "corrected" by the CPF to improve system stability monitoring.

The proposed method was able to detect that the system had moved into the alert state when the generator was tripped. Based on the results from the case study, it is not possible to conclude that the the actual maximum loadability of the system have been found by the proposed method.

Both CPF and SZ-I are based on simplifications of the real system. They are simplified in different ways, and to compare the resulting maximum loadability is in a way like comparing apples to oranges. CPF and S-ZI both overestimate the maximum loadability of the system, but the maximum loadability estimated from the S-ZI was found to be a lot more varying and less dependable. It is not possible to estimate correctly, due to the uncertainty of Z_{Th}, which can only accurately determined at the stability limit. Close to the stability limit, the S-ZI is a lot more applicable than CPF, which might not even be solvable if it comes too close.

A better estimation of the Z_{Th} is needed to make the proposed method more exact in regards of tracking the real maximum loading limit. The variation in the resulting $P_{MAX,S-ZI}$ is too big to give real information about the change in the maximum loadability in the proposed method. The result from the case study shows that the proposed method can, at best, provide an indication of where the system is moving, which for some purposes may be sufficient.

7 | Further Work

In terms of implementation:

- The tripping of the generator g18b, was not detected by the CPF. Further investigation on the CPF solution scheme by adding other types of "minor" contingencies should be done to test the implemented CPFs ability to track the maximum loadability in the system

- Improve the accuracy of the estimated Z_{Th} and the resulting maximum loadability $P_{MAX,S-ZI}$

- The X/R ratio changes with changed loading, implement something that can adapt to the change in the network. In practice, this imply that it is necessary to have some kind of communication between the PMU and the rest of the system

- Implementation of secondary voltage control that sets in when the algorithm detects that the system is in the alert state

- Run total solution scheme from Python

For the case study:

- Use of real system data

- Add load increase in other parts of the system to study the effect the the estimated $P_{MAX,REAL}$

- Add more reactive power reserves to investigate the effect on the maximum loadability

Bibliography

[1] P. Kundur, J. Paserba, V. Ajjarapu, G. Andersson, A. Bose, C. Canizares, and T. Van Cutsem. Definition and classification of power system stability ieee/cigre joint task force on stability terms and definitions. *IEEE transactions on Power Systems*, 19(3):1387–1401, 2004.

[2] L. H. Fink and K. Carlsen. Operating under stress and strain [electrical power systems control under emergency conditions]. *IEEE Spectrum*, 15(3):48–53, March 1978.

[3] P. Porbreik et al. Review of on-line dynamic security assessment tools and techniques. *CIGRE Technical Brochure, Paris*, 2007.

[4] J. De La Ree, V. Centeno, J. S. Thorp, and A. G. Phadke. Synchronized phasor measurement applications in power systems. *IEEE Transactions on Smart Grid*, 1(1):20–27, June 2010.

[5] U. Häger, C. Rehtanz, and N. Voropai. *Monitoring, Control and Protection of Interconnected Power Systems*, volume 36. Springer, 2014.

[6] G. N. Taranto, N. Martins, D. M. Falcao, A. C. B. Martins, and M. G. dos Santos. Benefits of applying secondary voltage control schemes to the Brazilian system. In *2000 Power Engineering Society Summer Meeting (Cat. No.00CH37134)*, volume 2, pages 937–942 vol. 2, 2000.

[7] J. Machowski, J. Bialek, and J. Bumby. *Power system dynamics: stability and control*. John Wiley & Sons, 2011.

[8] K. Vu, M. M. Begovic, D. Novosel, and M. M. Saha. Use of local measurements to estimate voltage-stability margin. *IEEE Transactions on Power Systems*, 14(3):1029–1035, Aug 1999.

[9] T. Van Cutsem and L. Papangelis. Description, modeling and simulation results of a test system for voltage stability analysis. Technical report, Université de Liège, 2013.

[10] PSS/E 33.0. *Program Operation Manual*. Siemens Energy, Inc., 2009.

[11] D. T. Duong. *Online Voltage Stability Monitoring and Coordinated Secondary Voltage Control*. PhD thesis, Norwegian University of Science and Technology, 2016.

[12] V. Rye-Holmboe. On-line stability assessment. Unpublished Specialisation Project, January 2017.

[13] J. Bian and P. Rastgoufard. Power system voltage stability and security assessment. *Electric Power Systems Research*, 30(3):197–201, 1994.

[14] N. Balu, T. Bertram, A. Bose, V. Brandwajn, G. Cauley, D. Curtice, A. Fouad, L. Fink, M. G. Lauby, B. F. Wollenberg, and J. N. Wrubel. On-line power system security analysis. *Proceedings of the IEEE*, 80(2):262–282, Feb 1992.

[15] V. Ajjarapu. *Computational techniques for voltage stability assessment and control.* Springer Science & Business Media, 2007.

[16] T. Van Cutsem and C. Vournas. *Voltage Stability of Electric Power Systems.* Springer Science & Business Media, 2007.

[17] T. Van Cutsem. Voltage instability: phenomena, countermeasures, and analysis methods. *Proceedings of the IEEE*, 88(2):208–227, Feb 2000.

[18] P. W. Sauer, K. L. Tomsovic, and V. Vittal. *Power System Stability and Control.* CRC press, 2nd edition, 2007.

[19] A. Abur and A. G. Exposito. *Power system state estimation: theory and implementation.* CRC press, 2004.

[20] A. G. Phadke and J. S. Thorp. *Synchronized phasor measurements and their applications.* Springer Science & Business Media, 2008.

[21] A. Gomez-Exposito, A. Abur, P. Rousseaux, A. de la Villa Jaen, and C. Gomez-Quiles. On the use of PMUs in power system state estimation. In *Proc. 17th Power Systems Computation Conference*, volume 22, page 26, 2011.

[22] M. Glavic and T. Van Cutsem. Wide-area detection of voltage instability from synchronized phasor measurements. part i: Principle. *IEEE Transactions on Power Systems*, 24(3):1408–1416, Aug 2009.

[23] S. Corsi. *Voltage control and protection in electrical power systems: from system components to wide-area control.* Springer, 2015.

[24] N. Martins. The new CIGRE task force on coordinated voltage control in transmission networks. In *2000 Power Engineering Society Summer Meeting (Cat. No.00CH37134)*, volume 1, pages 305–306 vol. 1, 2000.

[25] V. Ajjarapu and C. Christy. The continuation power flow: a tool for steady state voltage stability analysis. *IEEE Transactions on Power Systems*, 7(1):416–423, 1992.

[26] H. Chiang et al. CPFLOW: a practical tool for tracing power system steady-state stationary behavior due to load and generation variations. *IEEE Transactions on Power Systems*, 10(2):623–634, May 1995.

[27] H. Mori and S. Yamada. Continuation power flow with the nonlinear predictor of the lagrange's polynomial interpolation formula. In *Transmission and Distribution Conference and Exhibition 2002: Asia Pacific. IEEE/PES*, volume 2, pages 1133–1138 vol.2, Oct 2002.

[28] T. Gaddis. *Starting out with Python.* Pearson Addison Wesley, 3rd edition, 2009.

[29] R.D. Zimmerman, C.E. Murillo-Sánchez, et al. MATPOWER 6.0. `http://www.pserc.cornell.edu/matpower`, 2016.

A | Appendices

A.1 Dynamic Simulation in Python, in Detail

Runnig a Python Script and Initialise Working Case

The PSS/E 33 Command Promt have been used as the compiler for these simulations. The default direction for PSS/E 33 Command Promt is C\PTI\PSSE33\EXAMPLE. To run a Python file, it needs to be in the directed folder. To change direction to the folder with the files in it, the following had to be typed in:

```
>> cd C:\Users\vilder\MASTER
```

The PSS/E files must be added to path (line 1 to 5). The API routine returns an integer return code, where zero indicates success. When a non-zero value is returned (meaning that something did not work out as planned), other returned values are set to none in Python. To avoid this, Python must be set to throw exceptions instead of returning error code values (see line 7). Line 8 redirects the PSS/E output to Python.

```
1  psse_path = r"C:\PTI\PSSE33\PSSBIN"
2  folder = r"C:\Users\vilder\MASTER"
3  sys.path.append(psse_path)
4  sys.path.append(folder)
5  os.environ['PATH'] += ";" + psse_path
6
7  psspy.throwPsseExceptions = True
8  redirect.psse2py()
9
10 # Initialise working case:
11 psspy.psseinit(10000)
12 psspy.case(casefile)
13 psspy.dyre_new([1,1,1,1],dyrfile,"","","")
14 AddOutputChannelPMU.nhap()
```

After PSS/E have been initialised (line 11), a working case and a dynamic data file must be imported. Line 12 opens the PSS/E Saved Case (.sav) and transfer the data into the PSS/E working case. Line 13 clears the dynamics working memory and read dyrefile (.dyr) into dynamics working memory. AddOutputChannelPMU.nhap() is a Python file, that import the output channels of the system. Output channels for voltage magnitude and phase angle are given by

```
psspy.voltage_and_angle_channel(status, ident)
```

and for active and reactive power

```
psspy.load_array_channel(status, ident)
```

Input variables are given in Table A.1 and A.2. status(1) are not given a value, the order of output channels will follow the order in AddOutputChannelPMU.py. The measurements are used in the SZ-I, and therefor only necessary at BUS 1.

Table A.1: Input variables voltage_and_angle_channel()

Input variable	Type of input	Description
status(1)	Integer	Starting channel index (next available by default)
status(2)	Integer	Starting VAR index (next available by default)
status(3)	Integer	Starting ICON index (next available by default)
status(4)	Integer	Bus number
ident	Character	Array of two identifiers to assign the output channels

Table A.2: Input variables load_array_channel()

Input variable	Type of input	Description
status(1)	Integer	Starting channel index (next available by default)
status(2)	Integer	= 1, PLOAD = 2, QLOAD
status(3)	Integer	Load bus number
ident	Character	Array of two identifiers to assign the output channels

Dividing System into Subsystems

The power system can be divided into subsystems width valid subsystem ID's spanning from 0 to 11. To create a subsystem of one simple bus:

```
ierr = psspy.bsyso(sid, busnum)
```

where assigning the subsystem id (sid) to the wanted bus-number. Otherwise, subsystems of many buses can be sorted out by specifying an array of buses or an array of buses by the area, owner or zone number they belong to:

```
ierr = psspy.bsys(sid, usekv, basekv, numarea, areas, numbus, buses,
          numowner, owners, numzone, zones)
```

If the usekv is set to 0, basekv do not have to be assigned a value. Only one set of num* and * (*=areas, bus(es), owner or zones) needs to be assigned to form the subsystem. The variable ierr returns 0, if no error occurred, and 1, if the SID is invalid.

Table A.3: Input variables bsys()

Input variable	Type of input	Description
sid	Integer	Valid subsystem identifier (0-11)
usekv	Integer	= 0, use base kV = 1, do not use base kV
basekv(1)	Real number	Minimum base kV limit
basekv(2)	Real number	Maximum base kV limit
numareas	Integer	Total number of areas to include
areas	Array of integer(s)	Specify which area number(s) to include
numbus	Integer	Total number of buses to include
buses	Array of integer(s)	Specify which bus number(s) to include
numowner	Integer	Total number of owners to include
owners	Array of integer(s)	Specify which owner(s) to include
numzones	Integer	Total number of zones to include
zones	Array of integer(s)	Specify which zone number(s) to include

Run Dynamic Simulation

To API to run the PSS/E state-space dynamic simulations, is given by

```
pssspy.run(option, tpause, nprt, nplt, ctrplt)
```

with the input data given in Table A.4. The input variables option, nprt and crtplt have been left with their default settings. nplt is set to 4, in order to save data to the output file every 40 ms (which is the normal rate of data sent from the PMU). When the load is increased tpause is set to t=t+dt.

Table A.4: Input variables run()

Input variable	Type of input	Description
option	Integer	= 0, printed convergence monitor only if enabled by the CM interrupt control code (0 by default) = 1, automatically print convergence monitor limits
tpause	Real number	Time at which the simulation should next pause
nprt	Integer	Time steps between printing output values channel
nplt	Integer	Time steps between writing to the output channel
crtplt	Integer	Time steps between plotting values designated as CRT output channel

Save Working Case as Power Flow Raw Data file

The rawd_2 function replicate the current working case as a Power Flow Raw Data (.raw) file . The .raw-file contains "measurements" of the whole system and is used as input data to the continuation power flow in MATPOWER.

```
pssspy.rawd_2(sid, all, status, out, ofile)
```

Input variables that have to be set are given in Table A.5. SID is set to 0, all is set to 1 (process all buses) and *out* is set to 0, so that the output file is directed to the *ofile*. The array of *status* variables are set to default values (see table).

Table A.5: Input variables rawd_2()

Input variable	Type of input	Description
sid	Integer	Valid subsystem identifier (0-11)
all	Integer	= †n0, process all buses when status(4)= 0 process tie branches when status(4)= 1 = 1, process all buses in sid (by default)
status	Integer	Array of 7 integers, specifying output options. For status(1)-(4) and status(6): = 0, no = 1, yes
status(1)	Integer	Records of type 4 (1 by default)
status(2)	Integer	Records of out-of-service branches (1 by default)
status(3)	Integer	Records of equipment in SID (1 by default)
status(4)	Integer	Records of SID tie branches(0 by default)
status(5)	Integer	= 0, for subsystem loads at all buses (by default) = 1, subsystem loads at all buses = 2, all loads at subsystem buses and subsystem loads at non-subsystem buses
status(6)	Integer	Bus name as bus identifier (0 by default)
status(7)	Integer	=0, Raw data file type (by default)
out	Integer	= 0, direct output data file to ofile = 1, direct output data to progress window (1 by default)
ofile	Character ofile*260	Ouput file name

Add Load Increase

The general structure of SCAL is given below. First, the SID of the subsystem must be set, then it is defined whether all buses in system or only the bus(es) in the SID, should be processed.

```
ierr, totals, moto = psspy.scal(sid, all, apiopt, status, scalval)
```

scalval are used to set the scaling target, i.e. the specified total power, percent change or incremental powers depending on the value of status(1). A list of all input variables are given in Table A.6. scalval(2)-scalval(6) set the scaling target value in MW or MVAr for generation, shunts, reactors, capacitors and motor loads, and are not specified since the SCAL is only used to increase the load demand.

Table A.6: Input variables scal()

Input variable	Type of input	Description
sid	Integer	Valid subsystem identifier (0-11)
all	Integer	= 0, process all buses = 1, process only busses in the sid
apiopt	Integer	Mode of operation (0 by default) = 0, initialise for scaling, run scaling and post-process for scaling. = 1, initialise for scaling = 2, run the scaling and post-processing for housekeeping
status(1)	Integer	Scaling active power load, generation and motor data = 0, no scaling = 1, specify new total power = 2, specify percent changes = 3, specify incremental powers
status(2)	Integer	= 0, ignore machine power limits (by default) = 1, enforce machine power limits
status(3)	Integer	Scaling rule to be enforced when changing the reactive power load = 0, no change = 1, constant P/Q ratio = 2, new total Q load = 3, percentage change = 4, new power factor = 5, increment Q load
status(4)	Integer	Bus type code flag for scaling, only checked and saved when aiopt= 0 or 1 (0 by default) = 0, all buses in subsystem = 1, only type 1 buses in subsystem = 2, only type 2 or 3 buses in subsystem
scalval(1)	Real number	Load MW total/perecent/increment
scalval(7)	Real number	Reactive load scaling parameter

Add Contingency to Dynamic Simulation

For the two types of contingencies applied in the study cases, tripping of a machine and a line the following APIs have been used

```
pssspy.dist_machine_trip(ibus, id)
```

for tripping a machine at bus number *ibus* (integer) with machine id (Character id*2).

```
pssspy.dist_branch_trip(ibus, jbus, id)
```

for tripping of line between bus *ibus* and *jbus* (both integers) and circuit identifier (character id*2).

A.2 MATPOWER Functions

These tables are taken from [29], and more detailed information about the functions applied can be retrieved from there.

MATPOWER Case Struct

The .raw file is converted to a MATPOWER case struct (mpc) by:

```
mpc = psse2mpc(rawfile_name)

>> mpc
mpc =

  struct with fields:

    baseMVA: 100
        bus: [74x13 double]
   bus_name: {74x1 cell}
     branch: [102x13 double]
        gen: [21x25 double]
```

The mpc is a MATLAB struct that contains baseMVA, bus, bus name, branch and generator. baseMVA is a scalar, and the other values consists of a data matrices where each row correspond to a bus, a branch and generator. The corresponding content of each column is presented in Table A.7, A.8 and A.9.

name	column	description
BUS_I	1	bus number (positive integer)
BUS_TYPE	2	bus type (1 = PQ, 2 = PV, 3 = ref, 4 = isolated)
PD	3	real power demand (MW)
QD	4	reactive power demand (MVAr)
GS	5	shunt conductance (MW demanded at $V = 1.0$ p.u.)
BS	6	shunt susceptance (MVAr injected at $V = 1.0$ p.u.)
BUS_AREA	7	area number (positive integer)
VM	8	voltage magnitude (p.u.)
VA	9	voltage angle (degrees)
BASE_KV	10	base voltage (kV)
ZONE	11	loss zone (positive integer)
VMAX	12	maximum voltage magnitude (p.u.)
VMIN	13	minimum voltage magnitude (p.u.)
LAM_P[†]	14	Lagrange multiplier on real power mismatch (u/MW)
LAM_Q[†]	15	Lagrange multiplier on reactive power mismatch (u/MVAr)
MU_VMAX[†]	16	Kuhn-Tucker multiplier on upper voltage limit (u/p.u.)
MU_VMIN[†]	17	Kuhn-Tucker multiplier on lower voltage limit (u/p.u.)

[†] Included in OPF output, typically not included (or ignored) in input matrix. Here we assume the objective function has units u.

Table A.7: Bus Data (mpc.bus)

name	column	description
F_BUS	1	"from" bus number
T_BUS	2	"to" bus number
BR_R	3	resistance (p.u.)
BR_X	4	reactance (p.u.)
BR_B	5	total line charging susceptance (p.u.)
RATE_A	6	MVA rating A (long term rating), set to 0 for unlimited
RATE_B	7	MVA rating B (short term rating), set to 0 for unlimited
RATE_C	8	MVA rating C (emergency rating), set to 0 for unlimited
TAP	9	transformer off nominal turns ratio, (taps at "from" bus, impedance at "to" bus, i.e. if $r = x = b = 0$, $tap = \frac{|V_f|}{|V_t|}$)
SHIFT	10	transformer phase shift angle (degrees), positive $\Rightarrow$ delay
BR_STATUS	11	initial branch status, 1 = in-service, 0 = out-of-service
ANGMIN[*]	12	minimum angle difference, $\theta_f - \theta_t$ (degrees)
ANGMAX[*]	13	maximum angle difference, $\theta_f - \theta_t$ (degrees)
PF[†]	14	real power injected at "from" bus end (MW)
QF[†]	15	reactive power injected at "from" bus end (MVAr)
PT[†]	16	real power injected at "to" bus end (MW)
QT[†]	17	reactive power injected at "to" bus end (MVAr)
MU_SF[‡]	18	Kuhn-Tucker multiplier on MVA limit at "from" bus (u/MVA)
MU_ST[‡]	19	Kuhn-Tucker multiplier on MVA limit at "to" bus (u/MVA)
MU_ANGMIN[‡]	20	Kuhn-Tucker multiplier lower angle difference limit (u/degree)
MU_ANGMAX[‡]	21	Kuhn-Tucker multiplier upper angle difference limit (u/degree)

[*] Not included in version 1 case format. The voltage angle difference is taken to be unbounded below if ANGMIN < -360 and unbounded above if ANGMAX > 360. If both parameters are zero, the voltage angle difference is unconstrained.

[†] Included in power flow and OPF output, ignored on input.

[‡] Included in OPF output, typically not included (or ignored) in input matrix. Here we assume the objective function has units u.

Table A.8: Branch Data (mpc.branch)

name	column	description
GEN_BUS	1	bus number
PG	2	real power output (MW)
QG	3	reactive power output (MVAr)
QMAX	4	maximum reactive power output (MVAr)
QMIN	5	minimum reactive power output (MVAr)
VG	6	voltage magnitude setpoint (p.u.)
MBASE	7	total MVA base of machine, defaults to baseMVA
GEN_STATUS	8	machine status, $\begin{array}{l} > 0 = \text{machine in-service} \\ \leq 0 = \text{machine out-of-service} \end{array}$
PMAX	9	maximum real power output (MW)
PMIN	10	minimum real power output (MW)
PC1[*]	11	lower real power output of PQ capability curve (MW)
PC2[*]	12	upper real power output of PQ capability curve (MW)
QC1MIN[*]	13	minimum reactive power output at PC1 (MVAr)
QC1MAX[*]	14	maximum reactive power output at PC1 (MVAr)
QC2MIN[*]	15	minimum reactive power output at PC2 (MVAr)
QC2MAX[*]	16	maximum reactive power output at PC2 (MVAr)
RAMP_AGC[*]	17	ramp rate for load following/AGC (MW/min)
RAMP_10[*]	18	ramp rate for 10 minute reserves (MW)
RAMP_30[*]	19	ramp rate for 30 minute reserves (MW)
RAMP_Q[*]	20	ramp rate for reactive power (2 sec timescale) (MVAr/min)
APF[*]	21	area participation factor
MU_PMAX[†]	22	Kuhn-Tucker multiplier on upper P_g limit (u/MW)
MU_PMIN[†]	23	Kuhn-Tucker multiplier on lower P_g limit (u/MW)
MU_QMAX[†]	24	Kuhn-Tucker multiplier on upper Q_g limit (u/MVAr)
MU_QMIN[†]	25	Kuhn-Tucker multiplier on lower Q_g limit (u/MVAr)

[*] Not included in version 1 case format.
[†] Included in OPF output, typically not included (or ignored) in input matrix. Here we assume the objective function has units u.

Table A.9: Generator Bus (mpc.gen)

.

Continuation Power Flow

Function to run continuation power flow:

```
results = runcpf(basecasedata, targetcasedata, mpopt, fname, solvedcase);
```

Settings in the continuation power flow can be made by inserting directions in mopt (see Table A.10).

name	default	description
cpf.parameterization	3	choice of parameterization 1 — natural 2 — arc length 3 — pseudo arc length
cpf.stop_at	'NOSE'	determines stopping criterion 'NOSE' — stop when nose point is reached 'FULL' — trace full nose curve λ_{stop} — stop upon reaching target λ value λ_{stop}
cpf.step	0.05	continuation power flow step size
cpf.adapt_step	0	toggle adaptive step size feature 0 — adaptive step size disabled 1 — adaptive step size enabled
cpf.error_tol	10^{-3}	tolerance for the adaptive step controller
cpf.step_min	10^{-4}	minimum allowed step size
cpf.step_max	0.2	maximum allowed step size
cpf.plot.level	0	control plotting of nose curve 0 — do not plot nose curve 1 — plot when completed 2 — plot incrementally at each iteration 3 — same as 2, with **pause** at each iteration
cpf.plot.bus	*empty*	index of bus whose voltage is to be plotted
cpf.user_callback	*empty*	string or cell array of strings with names of user callback functions[†]
cpf.user_callback_args	*empty*	struct passed to user-defined callback functions[†]

Table A.10: Input variables for continuation power flow options, mopt

.

name	description
results.cpf.iterations	n_{steps}, number of continuation steps performed
results.cpf.lam_c	$1 \times n$ vector of λ values from correction steps[†]
results.cpf.lam_p	$1 \times n$ vector of λ values from prediction steps[†]
results.cpf.max_lam	maximum value of λ found in `results.cpf.lam_c`
results.cpf.V_c	$n_b \times n$ matrix of complex bus voltages from correction steps[†]
results.cpf.V_p	$n_b \times n$ matrix of complex bus voltages from prediction steps[†]

[†] n is one more than the number of continuation steps, i.e. $n_{\text{steps}} + 1$.

Table A.11: Continuation Power Flow Results

.

| name	description
Inputs	
k	continuation step iteration count
V_c	vector of complex bus voltages after k-th corrector step
lam_c	value of λ after k-th corrector step
V_p	vector of complex bus voltages after k-th predictor step
lam_p	value of λ after k-th predictor step
cb_data	struct containing potentially useful static data, with the following fields (all based on internal indexing):
.mpc_base	MATPOWER case struct of base state
.mpc_target	MATPOWER case struct of target state
.Sxfr	handle of function returning complex vector of scheduled power transfers in p.u. (difference between bus injections in base and target cases), b from (5.4)
.Ybus	bus admittance matrix
.Yf	branch admittance matrix, "from" end of branches
.Yt	branch admittance matrix, "to" end of branches
.pv	list of indices of PV buses
.pq	list of indices of PQ buses
.ref	list of indices of reference buses
.mpopt	MATPOWER options struct
cb_state	user-defined struct containing any information the callback function would like to pass from one invokation to the next
cb_args	callback arguments struct specified in cpf.user_callback_args
results	initial value of output struct to be assigned to cpf field of results struct returned by runcpf
Ouputs	
cb_state	updated version of cb_state input argument
results	updated version of results input argument

Table A.12: Continuation Power Flow runcpf() Callback Arguments

A.3 Extended-Term Load Reset (EXTL) Model

The Extended-Term Load Reset (EXTL) Model can be found in the PSS/E model library in [10], and it is added to simulate load restoration in the system. The EXTL Model resets the loads to constant active and reactive power loads in steady-state. No other specific modelling of the equipment is necessary. The block diagram of the EXTL model is presented in Figure A.1 for both active and reactive power consumed by the load.
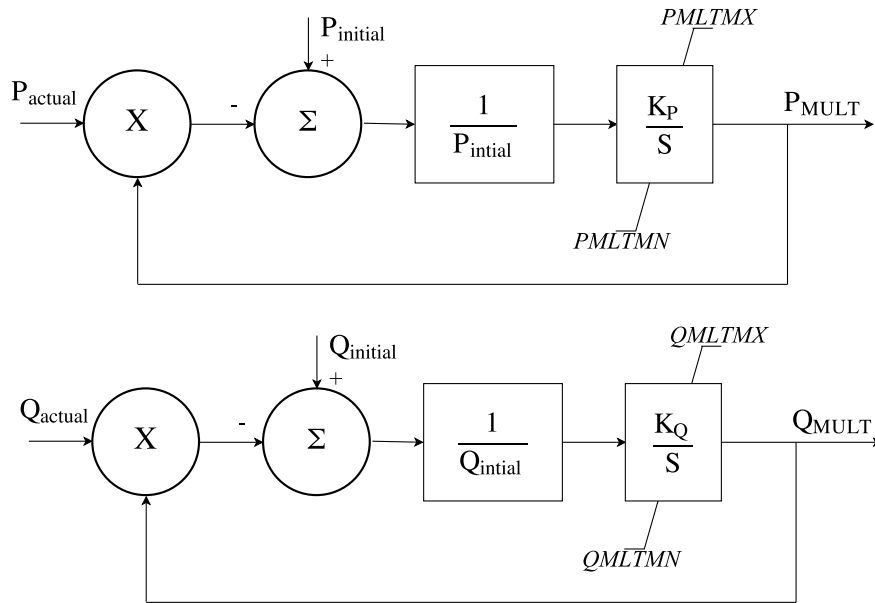
Figure A.1: Extended-Term Load Reset Model [10]

The actual load is fed into the model and summarised with the current controlled load increase P_{MULT} and Q_{MULT}. Then the power mismatch, compared to the $P_{initial}$ is found. To find the power mismatch the sum of nominal power is subtracted, and the total mismatch from compared to the intial loading is found. To this value, a gain of K_P and K_Q is multiplied, and the EXTL model allows output P_{MULT} within the limits of $PMLTMX$ and $PMLTMN$. The settings applied to the model are presented in Table A.13 below.

Table A.13: Settings applied to the Extended-Term Load Reset Model

K_P	$PMLTMX$	$PMLTMN$	K_Q	$QMLTMX$	$QMLTMN$
0.02	2.00	-2.00	0.02	2.00	-1.00